Applied Geochemistry 168 (2024) 106028

Contents lists available at ScienceDirect

Applied Geochemistry

journal homepage: www.elsevier.com/locate/apgeochem

Geological and anthropogenic contributions of metal(loid)s in the artisanal and small-scale mining-impacted Ocoña watershed of Arequipa, Peru

Isaac J.P. Simon [a], Katharina Pfaff [a,*], Alexis Navarre-Sitchler [a,b], Jorge Crespo [c,1], Elizabeth Holley [c], Gary Vanzin [d], Madeleine N. Guillen Gomez [e], Sergio Ticona-Corrales [e], Jonathan O. Sharp [b,d]

[a] Department of Geology and Geological Engineering, Colorado School of Mines, USA
[b] Hydrologic Science and Engineering Program, Colorado School of Mines, USA
[c] Department of Mining Engineering, Colorado School of Mines, USA
[d] Department of Civil and Environmental Engineering, Colorado School of Mines, USA
[e] Centro de Minería Sostenible, Universidad Nacional de San Agustín de Arequipa, Peru

ARTICLE INFO

Editorial handling by: JoAnn M Holloway

Keywords:
Arequipa
Acid mine drainage
Metal mobility
Water quality

ABSTRACT

Strategies to resolve conflicts around water supply and quality in mining-impacted communities include a better understanding of the role and mitigation of mining activities proximal to surface water bodies. The Ocoña watershed of Arequipa (Peru) is one such region where there are conflicts between artisanal miners, fishers, and agriculture over local water resources. The aim of this study is to develop a workflow that leverages existing water quality monitoring and geological mapping to identify major processes that adversely impact water quality with a focus on the relative contribution of mining-related activities on the Ocoña watershed. This study integrates a statistical evaluation of water chemistry data, concentration-discharge relationships, and detailed mineralogy with geochemical modeling to identify sources and mechanisms of contaminant contributions to surface waters in the Ocoña watershed. This revealed that primary deposit mineralogy and seasonal variations exert direct effects on water quality in this mining-active watershed. Multivariate statistical analysis reveals two distinct hydrogeochemical signatures in Ocoña River water that likely represent natural geothermal activity in the northern portion and acid mine drainage contribution in the southern portion of the watershed. In both cases, anthropogenic activities such as mining and agricultural may increase contaminant mobilization. Interestingly, despite perceived challenges, water quality in the Ocoña watershed is better than that of neighbors potentially due to pH-controlled precipitation of Fe and resultant sorption of metals onto precipitants. However, copper released from acid mine drainage, and in particular peak concentrations during the high flow season, exert a potential for adverse ecotoxicological effects. This workflow could potentially be extrapolated to other regions with similar available data to better identify the relative contributions of natural and anthropogenic pressures to the release of toxic compounds in watersheds of concern.

1. Introduction

In the state of Arequipa in southern Peru, community concerns surrounding mining and mining related activities are predominantly focused on water supply and quality. Although large scale mining is present in Arequipa (e.g. Cerro Verde), artisanal and small-scale mining (ASM) represents a significant form of mining activity in the region. In the semi-arid Arequipa region, as in far wetter regions such as the Surinamean rainforest (Lewis et al., 2020), increasing ASM activity has been blamed for negatively impacting water quality. In the Ocoña watershed of Arequipa, water-related issues have led to contention due to concerns of ASM impacting other livelihoods like fishing (Malone et al., 2021). In the Ocoña River, locals attribute the decline in shrimp population to growing mining activity in the area (Malone et al., 2021). Alongside threats to water quality, Arequipa watersheds face threats to the available quantity of this resource. Climate change models predict a

* Corresponding author.
E-mail address: kpfaff@mines.edu (K. Pfaff).
[1] Current address: Nevada Bureau of Mines and Geology, University of Nevada, Reno, USA.

https://doi.org/10.1016/j.apgeochem.2024.106028
Received 20 October 2023; Received in revised form 28 March 2024; Accepted 25 April 2024
Available online 26 April 2024

reduction in overall river discharge and water availability in the Ocoña watershed as increasing temperatures and reduced precipitation are projected to particularly impact water storage during winter months (Lasage et al., 2011). Future water resource insecurity leads to concerns across agricultural, fishery, mining, and other sectors. Therefore, identifying environmental and geochemical factors that influence surface water quality in specific watersheds is important to address water contamination concerns.

The aim of this study is to identify processes that contribute to water contamination as well as natural remediation processes within the Ocoña watershed, which serves as an example of a mining-active region in the state of Arequipa that is experiencing ongoing water-related disputes. Chemical and physical water parameters, physical and seasonal basin characteristics, information on anthropogenic activities, and mineralogical data of ore and tailings were integrated to determine hydrogeochemical signatures in the Ocoña watershed and to identify environmental influences on those signatures. Geochemical modeling was applied to determine the mineral reactions and processes responsible for contaminant contribution to river water. In this study a workflow to investigate metal(loid) contributions from different sources is applied to the Ocoña watershed. Insights of this work and the designed workflow can be applied toward other watersheds to improve our understanding of what sources and processes contribute to declining water quality through solute transport.

2. Methods and workflow

A compilation of water data from the literature was used to establish quality and composition of water in the Ocoña, through use of chemical parameters. Alongside chemical parameters, physical basin and water parameters were collected to evaluate other controls on water quality, such as river discharge, elevation and seasonal variations. Trends in water data, identified using statistical methods, were used to delineate groups of chemical parameters that are related to hydrogeochemical signatures. For mining-active regions, defining the detailed mineralogical characteristics of representative deposits and tailings supports an in-depth understanding of the water-rock interactions that are related to water contamination and natural remediation processes.

2.1. Sampling strategy

To improve our understanding of the impact of the geology and mining related activities on the water quality in the Ocoña watershed in southwest Peru, ore samples, host rock, and tailings from the San Juan de Chorunga mine were sampled for mineralogical characterization and calculation of mineral modal abundances. Thin sections of ore veins that were texturally and mineralogically characterized in Crespo et al. (2020), were used and re-analyzed for this study. The tailings pile was sampled at 15 spot locations, with a 20 m spacing, and at approximately 40 cm depths for a comprehensive sampling strategy. All samples were analyzed using field emission scanning electron microscopy (FE-SEM) and automated mineralogy to determine the mineral modal abundances of the San Juan de Chorunga deposit, host rock, and tailings while building on the mineralogical information previously documented.

2.2. Mineralogical analysis

Backscattered electron (BSE) images of tailings samples were captured using a TESCAN MIRA3 LMH Schottky Field Emission Scanning Electron Microscope (FE-SEM) in the Mineral and Materials Characterization (MMC) facility in the Department of Geology and Geological Engineering at the Colorado School of Mines in Golden, Colorado. The FE-SEM was operated at a working distance of 10 mm, a beam intensity of 11 and an acceleration voltage of 15 kV. Mineral identification was done through semi-quantitative analyses using a Bruker XFlash® 6/30 silicon drift energy dispersive x-ray spectrometer (EDS) operated with the Quantax Espirit software.

Automated mineralogy was carried out using a TESCAN Integrated Mineral Analyzer (TIMA) in the MMC Facility in the Department of Geology and Geological Engineering at the Colorado School of Mines. Thin sections of rock samples and ore, and an epoxy mount (tailings) were loaded into a TESCAN-VEGA-3 LMU variable pressure SEM platform that is equipped with two EDAX silicon drift EDS detectors and operated using the TIMA control program. The system was operated at a beam intensity of 14, an accelerating voltage of 25 kV and a stepping-size (resolution) of 15 μm. The EDS spectra from each acquisition point were compared with a look-up table of saved spectra for consecutive mineral/phase assignment and results were output by the TIMA software.

2.3. Synthesis of water chemistry data

Water quality and associated chemical data on the Ocoña watershed were compiled from the National Water Authority of Peru (SI Table 1; ANA, 2013a; ANA, 2014a; ANA, 2015a) and are described in Regis et al. (2022). The National Water Authority (ANA) collected data over three projects performed in: November–December 2012, November 2013, and March–April 2014. The compiled data represent a sparse dataset with analytes not consistently available. The dataset is also left-censored, with about 18% of analyte measurements that are below the limit of detection. Therefore, data processing steps for proper statistical calculations were carried out in the MATLAB programming and numeric computing platform. Variables that are dominantly (>50%) below detection limit or that contain excessive amounts of unreported values (>50%) are excluded from further statistical work. About 11% of river discharge data and 2% of pH data are unreported values, which were imputed with the mean of variable. Approximately 7% of data are left-censored (93% uncensored), after exclusion of variables that are dominantly (>50%) below detection limit or contain dominantly (>50%) unreported values. The left-censored values in the remaining variables were imputed by half of the limit of detection which affected Al (4% censored data), As (23% censored data), Ba (9% censored data), B (7% censored data), Cu (47% censored data), Li (14% censored data), Mn (2% censored data), Pb (18% censored data), and Total Suspended Solids (18% censored data). Imputation of left-censored data by half of the detection limit is expected to introduce bias and higher variability in a dataset, compared to parameter estimating methods like the Maximum Likelihood Estimate (MLE) and the Kaplan-Meier method (Helsel, 2005). Adjei and Stevens (2022) show imputation by half of the detection limit can outperform such methods in certain datasets by yielding lower bias. This approach is largely recommended for datasets that contain <15% below detection limit data (U.S. Environmental Protection Agency, 2000; U.S. Environmental Protection Agency, 2009). Therefore, an MLE was performed on left-censored variables to estimate mean and standard deviation by fitting data to a log-normal distribution, using MATLAB code in Bantis (2024). Comparison of MLE-calculated parameters and parameters from imputation methods show negligible differences, mostly within <5% error, except for Cu standard deviation (SI Table 2). A log10 transformation was applied to the dataset, omitting pH, which was followed by z-scored normalization. Following data transformation and normalization, a Principal Component Analysis (PCA) was applied to the following constituents of the Ocoña dataset: Al, As, Ba, B, Ca, Discharge, Cu, Fe, Li, Mg, Mn, Na, Total Suspended Solids, Temperature, Dissolved Oxygen, pH, and Pb. A supplementary Principal Component Analysis was calculated to explore the effects of Cu imputation by half of the detection limit due to the differences in standard deviation found in SI Table 2. Left-censored Cu data were randomly imputed by values below the highest detection limit in Cu, which does not show substantial changes in statistical relationships compared to imputation by half of detection limits (SI Table 3).

Bivariate statistics (correlation coefficient evaluations) and nonparametric comparative statistical tests (Kruskal-Wallis test) were

carried out with consideration of natural and anthropogenic influences on the hydrogeochemistry. Natural and anthropogenic influences on the hydrogeochemistry were investigated by evaluating data by categorical parameters: 1) elevation, 2) season, 3) rock type and 4) anthropogenic activities.

2.4. Concentration-discharge analysis

Concentration-discharge (CQ) relationships were quantified for the variables used in multivariate statistical observations. These relationships provide insights on chemical weathering and solute transport in a

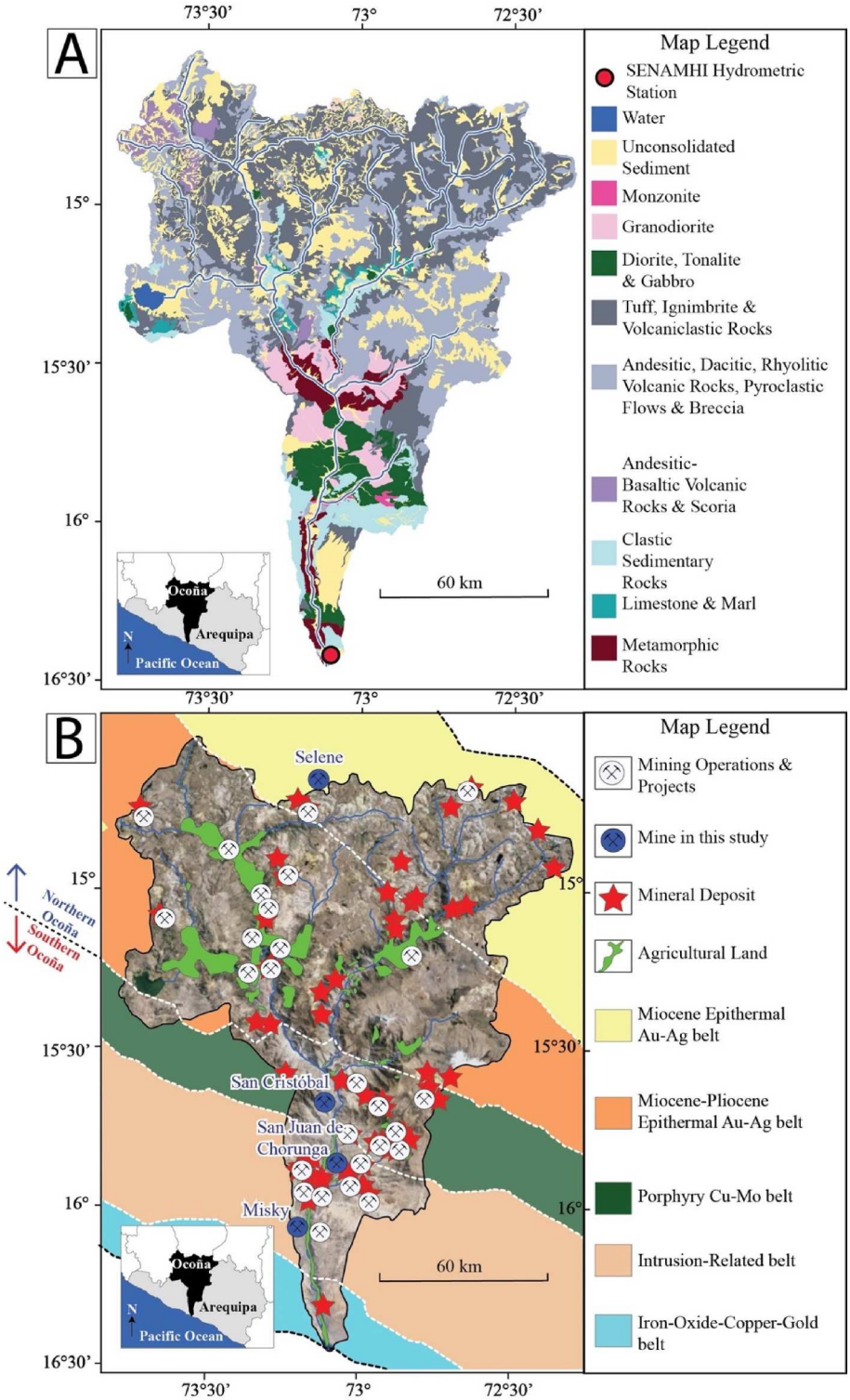

Fig. 1. Maps of the Ocoña watershed in Arequipa, southern Peru. A) Geologic map of the Ocoña watershed modified from Medina et al. (2021). B) Anthropogenic map of the Ocoña watershed showing the spatial distribution of agricultural activity and highlighting mining operations, both active and inactive. Also included are the known mineral deposits in the watershed and metallogenic belts as defined by Quispe et al. (2008). Deposits referenced and described in this study are highlighted in blue: Selene, San Cristóbal, San Juan de Chorunga, and Misky. The northern and southern sections of the Ocoña watershed are divided based on geologic characteristics and mineral deposit types. Spatial data are compiled from the Institute of Mining, Geology and Metallurgy (Hanco Mamani, 2010).

catchment (Godsey et al., 2009). The power law relation (*b*) established in Godsey et al. (2009) shows that the slope between log concentration and log discharge parameters can be used to quantify flushing, dilution, and chemostatic behavior. Chemostatic behavior is defined as conditions when the concentration of an analyte in solution is not dependent on variations of river discharge. In flushing systems, the concentration increases as discharge increases; conversely, dilution behavior is exhibited when concentrations decrease with increasing discharge. Thompson et al. (2011) propose a nonparametric measure of these varying C-Q behaviors defined by the ratio between the coefficients of variation for concentration and discharge data. The coefficient of variation ratio is calculated using the standard deviation of a variable, normalized by its mean (Thompson et al., 2011), and computed as follows:

$$CV_C/CV_Q = \mu_Q/\mu_C \bullet \sigma_C/\sigma_Q \quad (1)$$

Where CV is the coefficient of variation, μ is the mean, and σ is the standard deviation, for the analyte concentration (C in ppm) and discharge (Q in l/sec). Musolff et al. (2015) utilize both the power law relation (*b*; Godsey et al., 2009) and the coefficients of variation (CV_C/CV_Q; Thompson et al., 2011) to graphically display concentration-discharge relationships. Following the characterization scheme in Hoagland et al. (2020), solutes are characterized as chemostatic if $b \leq \pm 0.1$ and $CV_C/CV_Q \leq 0.2$. Chemodynamic behavior is characterized when $CV_C/CV_Q > 0.1$, where flushing is attributed with solutes with a positive *b* value and dilution is attributed with solutes with a negative *b* value. However, situations where data variance for solutes is significantly greater than discharge data variance, non-systematic CQ behavior is invoked.

2.5. Geochemical modeling

Thermodynamic modeling was done in Geochemist's Workbench® 2022 software package (Bethke, 2007). The Act2 application was used to create Eh-pH diagrams at temperature conditions reflective of the Ocoña watershed (18 °C) and at pressures of 1 bar. The following input metal concentrations were used to calculate activity values in thermodynamic modeling, based on maximum metal concentrations observed in the Ocoña watershed: 2.87 mg/L Fe, 3.28 mg/L Al, 2.63 mg/L Mn, and 0.03 mg/L Cu. The thermodynamic database used for phase stability calculations is the Lawrence Livermore National Laboratory (LLNL) thermos database. Electron activity values (Eh) were calculated using dissolved oxygen data from the Ocoña watershed dataset, based on the following redox half-reaction: $H_2O = ½\ O_2 + 2H^+ + 2e^-$.

3. The Ocoña watershed: physical, chemical, and anthropogenic attributes

3.1. Physiography and climate

The Ocoña watershed is a major river basin in southwest Peru that drains into the Pacific Ocean from the Andes Mountains (Fig. 1). It is located between latitudes of 14°30′S and 16°30′S, and between longitudes of 72°W and 74 °W (Fig. 1). The watershed covers approximately 16,000 km^2 and largely lies within the state of Arequipa, with sections of the northern basin located in the states of Ayacucho and Apurimac (Medina et al., 2021). Climatic features of the watershed vary by season and by elevation. The lowest seasonal temperatures in the region are experienced between May and November, roughly corresponding to the winter and spring months in the southern hemisphere with higher temperatures between December and April (Medina et al., 2021). Elevation also influences the average temperature in the watershed, demonstrated by water measurements across stations located at about 60 m.a.s.l. through 3200 m.a.s.l. (mean elevation = 2360 m.a.s.l.; Instituto Nacional de Recursos Naturales, 2007; Medina et al., 2021). Mean annual temperatures range between about 13 and 20 °C with lower temperatures being associated with higher elevations (>3000 m.a.s.l.) and higher temperatures being associated with lower elevations (60–2900 m.a.s.l.; Instituto Nacional de Recursos Naturales, 2007; Medina et al., 2021). Annual precipitation ranges between about 1 and 700 mm/yr with the greatest precipitation values observed at higher elevations (>3000 m.a.s.l.) and in the summer (Instituto Nacional de Recursos Naturales, 2007). River discharge values from the Servicio Nacional de Meteorología e Hidrología (SENAMHI) hydrometric station (Fig. 1) shows differences in river flow, dependent on months of the year in the Ocoña watershed (Instituto Nacional de Recursos Naturales, 2007; Medina et al., 2021). Peak river flows measured at the SENAMHI hydrometric station occur between January and May with an average annual flow between 90 and 300 m^3/s (Instituto Nacional de Recursos Naturales, 2007). The lowest river flow is observed between June and December with annual discharge values of about 50–70 m^3/s (Instituto Nacional de Recursos Naturales, 2007; Medina et al., 2021).

3.2. Geology, mineralogy, and ore deposits

The main lithologic units in the Ocoña watershed can generally be grouped into: (1) metamorphic rocks, (2) sedimentary rocks, (3) volcano-sedimentary rocks, (4) volcanic rocks, (5) intrusive rocks, and (6) unconsolidated sediments (Medina et al., 2021).

(1) Metamorphic rocks include gneiss, schist and phyllite (Medina et al., 2021, Fig. 1A) belonging to the Arequipa Massif, the Precambrian basement of the area that underlies the present-day arc and Western Cordillera (Shackleton et al., 1979; Boekhout et al., 2013).
(2) The sedimentary rocks in the basin consist of sandstone, shale, siltstone, conglomerate, limestone and marble (Medina et al., 2021, Fig. 1A).
(3) The volcano-sedimentary rocks are characterized by clastic sedimentary rocks interbedded with volcanoclastic rocks. Rock types include tuffaceous sandstone, conglomerate and interstratified volcanic rocks and breccias (Medina et al., 2021, Fig. 1A).
(4) The volcanic rocks in the basin are sourced from a multitude of volcanoes in the region including, but not limited to, the Sara Sara, Achatahua and Firura stratovolcanoes (Medina et al., 2021). Rock types include tuff, ignimbrite, andesite, dacite, trachyandesite, rhyolite, andesitic basalt and scoria (Medina et al., 2021, Fig. 1A).
(5) The intrusive rocks are stocks and hypabyssal intrusions of granodiorite, monzonite, diorite, tonalite and gabbro (Medina et al., 2021, Fig. 1A).
(6) Unconsolidated sediments consist of weakly- to non-consolidated material deposited during the Quaternary (Medina et al., 2021, Fig. 1A). Sedimentary material varies in depositional setting, namely fluvial, alluvial, colluvial, lacustrine, glacial, and aeolian deposits.

The volcanic rocks (4) are most prevalent in the Ocoña, covering more than 50% of the total basin surface area (Medina et al., 2021). This group of rocks predominantly occurs in the northern part of the Ocoña watershed (Fig. 1A), which corresponds to higher elevations and an Andean climatic setting. Excluding any unconsolidated sediments, the southern, arid-desert part of the basin is dominated by metamorphic rocks (1), intrusive rocks (5) and sedimentary rocks (2), which collectively cover approximately 20% of the total basin surface area (Medina et al., 2021, Fig. 1A).

The various rock types in the Ocoña watershed are host to approximately 60 known mineral deposits (Fig. 1B). Quispe et al. (2008) recognized that deposit types cluster spatially and defined metallogenic belts that are characterized by a predominant deposit type and

mineralization age.

A. The northern portion of the Ocoña features the Miocene Epithermal Au–Ag Belt and the Miocene-Pliocene Epithermal Au–Ag Belt, which collectively host slightly less than half of the known mineral deposits (n = 30) in the basin (Fig. 1B; Hanco Mamani, 2010). The Miocene-Pliocene Epithermal Au–Ag Belt (orange-colored belt in Fig. 1B) is host to high sulfidation epithermal deposits that formed in association with magmatic activity during the Miocene-Pliocene (Quispe et al., 2008; Acosta et al., 2010). There is one low sulfidation epithermal deposit and one intermediate sulfidation epithermal deposit located in this belt (Quispe et al., 2008; Acosta et al., 2010). The Miocene Epithermal Au–Ag Belt (yellow-colored belt in Fig. 1B) is host to high, low and intermediate sulfidation epithermal deposits with Au–Ag (Pb–Zn–Cu) metal affinities, including polymetallic Pb–Zn–Ag deposits overprinted by epithermal mineralization (Quispe et al., 2008; Acosta et al., 2010). There is a lack of detailed mineralogical studies on the Miocene epithermal deposits in northern Ocoña (yellow-colored belt in Fig. 1B). However, comprehensive petrographic and mineralogical work was done in the Selene mining district which exhibits low, intermediate, and high sulfidation epithermal mineralization styles (Dietrich et al., 2005; Palacios, 2006; Palacios et al., 2008; Sucapuca, 2019) and is located <5 km north of the Ocoña watershed boundary (Fig. 1B; Fig. 2). Deposits in the Selene mining district are hosted in intermediate to felsic volcanic and volcaniclastic rocks (see Sucapuca, 2019). Alteration mineral assemblages include alunite-pyrophyllite-dickite-kaolinite in the advanced argillic zones, smectite-illite-sericite-kaolinite-adularia in the intermediate argillic zones, and chlorite-calcite-smectite-pyrite-epidote in the propylitic zones (Sucapuca, 2019). Silicification results in ocherous quartz, silica replacement and chalcedony (Palacios, 2006; Sucapuca, 2019). Ore minerals include Ag sulfosalts with minor Cu sulfosalts and few sulfides including chalcopyrite, galena, sphalerite, arsenopyrite, bornite, marcasite, pyrite, digenite and covellite (Sucapuca, 2019 and references therein).
B. The southern portion of the watershed hosts slightly over half (n = 32) of the known mineral deposits in the Ocoña, 16 of which are located in the Porphyry Cu–Mo Belt (green-colored belt in Fig. 1B), 15 in the Intrusion-related Deposits Belt (cream-colored belt in Fig. 1B) and only one in the Iron-Oxide-Copper–Gold Belt (blue colored belt; Fig. 1B; Hanco Mamani, 2010). The Porphyry Cu–Mo Belt (green-colored belt in Fig. 1B) is predominantly characterized by Cu–Mo mineralization, but is also host to the San Cristóbal Intrusion-related deposit. The porphyry Cu–Mo deposits are related to emplacement of Late Cretaceous granitoids (Quispe et al., 2008), although causative intrusions have varying emplacement ages (e.g. Eocene at Don Javier, Ye et al., 2022; early Jurassic at Zafranal, Santos et al., 2019). Detailed literature on the mineralogy of these porphyry Cu–Mo deposits in the Ocoña is lacking, but neighboring Arequipa watersheds feature large well-studied deposits along the same metallogenic belt, such as Zafranal, which is located in the Camaná-Majes-Colca watershed (Camaná; Fig. 2; Hanco Mamani, 2010), as well as Don Juan and Cerro Verde-Santa Rosa, which are located in the Quilca-Vitor-Chili watershed (Chili; Fig. 2; Hanco Mamani, 2010)). The three deposits share potassic, sericitic/phyllic and propylitic alteration styles as main alteration types in and around porphyry Cu–Mo mineralization (Quang et al., 2003; Santos et al., 2019; Ye et al., 2022). Potassic alteration assemblages mainly include orthoclase and biotite where hypogene mineralization is present (Quang et al., 2003; Santos et al., 2019; Ye et al., 2022). Phyllic/sericitic alteration consists of quartz, sericite and pyrite at Zanfranal and Cerro Verde-Santa Rosa, whereas at Don Javier this alteration type additionally includes illite and smectite (Quang et al., 2003; Santos et al., 2019; Ye et al., 2022). Propylitic alteration is described as widespread, as well as occurring in an envelope and as a halo around all three aforementioned porphyry Cu–Mo deposits (Quang et al., 2003; Santos et al., 2019; Ye et al., 2022). At Zafranal, the propylitic alteration assemblage is composed of epidote and chlorite (Santos et al., 2019), whereas Don Javier exhibits propylitic alteration that consists of chlorite, epidote, and calcite (Ye et al., 2022). Furthermore, Ye et al. (2022) describe a chloritic-sericitic alteration zone overprinting the potassic alteration zone which is often spatially associated with higher Cu and Mo grades. Hypogene mineralization includes veins or breccias containing chalcopyrite,

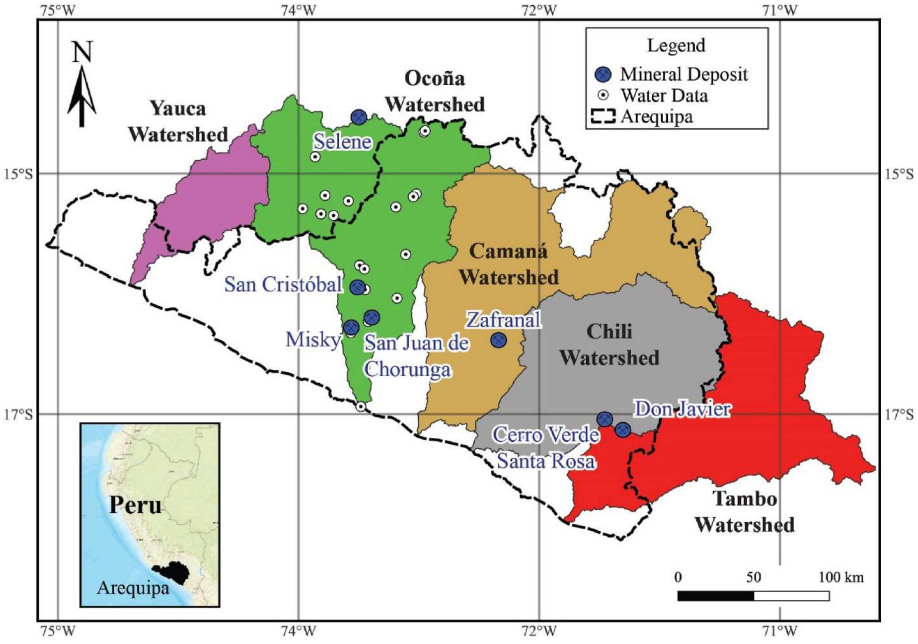

Fig. 2. Map of the department of Arequipa highlighting the five major watersheds in the state. Sample sites for compiled physicochemical water data parameters (temperature, conductivity, discharge, water chemistry) considered in this study are overlain on the map. Location of mineral deposits that are described in this study are highlighted in blue: Selene, San Cristóbal, Misky, San Juan de Chorunga, Zafranal, Cerro Verde-Santa Rosa and Don Javier. Spatial data of mineral deposits and watershed boundaries are from the Institute of Mining, Geology and Metallurgy (Hanco Mamani, 2010).

pyrite and gangue minerals (Quang et al., 2003; Santos et al., 2019; Ye et al., 2022). The main supergene mineral described across the three deposits is chalcocite, however chalcanthite, malachite, chrysocolla, neotocite, covellite and brochantite are described in at least one of the three deposits (Quang et al., 2003; Santos et al., 2019; Ye et al., 2022). Host rocks to mineralization are either granitoid rocks (e.g. dacite, diorite, quartz diorite) or Precambrian orthogneiss of the Arequipa Massif (Quang et al., 2003; Santos et al., 2019; Ye et al., 2022). The Intrusion-related Au–Pb–Zn–Cu Belt (cream-colored belt in Fig. 1B) is characterized by quartz-gold-sulfide mineralized structures hosted in Late Cretaceous granitoids (Quispe et al., 2008; Acosta et al., 2010). Detailed mineralogical studies of intrusion-related vein deposits at the Ocoña have been done on San Juan de Chorunga, Misky and San Cristóbal (Fig. 1B; Fig. 2; Palacios et al., 2011; Palacios et al., 2014; Alfonso et al., 2019; Crespo et al., 2020). Despite falling within the Porphyry Cu–Mo Belt, the San Cristóbal deposit was characterized as an intrusion-related gold deposit through detailed mineralogical studies (see Alfonso et al., 2019). Intrusion-related gold veins are typically less than 1 m thick and are composed of quartz, calcite, chlorite, sericite and pyrite (Palacios et al., 2011; Alfonso et al., 2019; Crespo et al., 2020). Although pyrite is the dominant sulfide phase, other common sulfides include chalcopyrite, sphalerite and galena, which are present in minor amounts. Precious metals occur as native gold or electrum with associated alteration halos characterized by sericitization, chloritization and silicification (Palacios et al., 2011, 2014; Alfonso et al., 2019; Crespo et al., 2020). Quartz is the dominant gangue mineral with calcite abundances being variable between deposits. In some deposits (i.e., Misky), calcite is minimal or rare (Palacios et al., 2011), whereas at San Juan de Chorunga, calcite is an abundant gangue mineral (Crespo et al., 2020). The rocks hosting these intrusion-related gold veins are felsic-to intermediate-intrusive igneous rocks including granodiorite, diorite and quartz monzonite (see Palacios et al., 2011; Palacios et al., 2014; Alfonso et al., 2019; Crespo et al., 2020).

3.3. Anthropogenic activity and potential for conflict

Along river valleys in the Ocoña basin, flood plains and terraces are used for farming (Santi et al., 2021, Fig. 1B), primarily cultivating rice, beans, maize, alfalfa and fruit trees (Medina et al., 2021). Fishing activities are focused on harvesting the freshwater crustacean *camarones de río* or river shrimp within the Ocoña river by hand and small traps (Malone et al., 2021; Medina et al., 2021; Santi et al., 2021). Fishing takes place mainly during the fall, winter and spring months of March through December (Medina et al., 2021). Alongside fishers and farmers in the river valleys, miners exploit mineral deposits like the gold-bearing quartz veins of the southern Ocoña (Intrusion-related Au–Pb–Zn Cu Deposits Belt; Fig. 1B) some of which have been mined since 1897, though it is believed that extraction took place in the colonial era (Costa et al., 2009; Malone et al., 2021), taking place as early as 1536 in Arequipa through Spanish settlement (Cuadros, 2022). Since the early 2000's, artisanal and small-scale mining activities have increased significantly and have become a prominent anthropogenic activity alongside fishing and farming, resulting in an influx of population into the river valley (Malone et al., 2021). Increasing mining-related activities have led to conflicts due to concerns of mining impacting water quality and availability (Brain, 2017). According to Malone et al. (2021), the availability of water used in mining for mineral processing does not appear to be an issue in the Ocoña basin, leaving plenty for agriculture and domestic water use. However, concerns that mining is impacting the water quality were noted in public interviews and surveys (Malone et al., 2021), highlighting fears of effects to the population of river shrimp. River water contamination concerns are warranted as there is documentation of Hg contamination from mineral processing in artisanal and small-scale mining along the Ocoña watershed (Costa et al., 2009; Smith, 2019). Moreover, the detrimental impacts of mining to the environment are known from other parts of the world as mine drainage has been responsible for the death of abundant fish, benthic organisms and crops as well as has harmed livestock and rendered rivers unfit for other anthropogenic activities (Nordstrom and Alpers, 1999). Mining and mineral processing can result in acid mine drainage through sulfide oxidation in a variety of mining by-products such as tailings, waste rock, leach pads and slag, mobilizing contaminants to nearby waters (Nordstrom and Alpers, 1999; Nordstrom et al., 2015). Tailings, in particular, are commonly responsible for river water contamination across the globe (e.g. Mexico; Armienta et al., 2004; Italy; Concas et al., 2006; Uganda; Abraham and Susan, 2017; China; Liang et al., 2017). Artisanal and small-scale mining operations in the Ocoña watershed do not store tailings locally as mined ore material is sold to distant plants to be reprocessed with cyanide for additional gold extraction (Malone et al., 2021). However, the medium-scale Century Mining Company Peru S.A.C. stores tailings locally in the watershed at the San Juan de Chorunga gold mine where cyanide is used to process material (Crespo et al., 2020; Malone et al., 2021). Moreover, other mining by-products, such as waste rock piles, are kept at ASM operation sites in the Ocoña watershed and can also contribute contamination when disposed rock enters the river (Malone et al., 2021) or when low water quality drainage is developed from meteoric water interacting with waste rock piles (see Nordstrom et al., 2015).

4. Results and discussion

4.1. Water chemical parameters of the Ocoña watershed

A summary of select variables describing the characteristics of surface water in the Ocoña watershed is shown in Table 1. Summary statistics compared to Peruvian water quality standards (Ministerio del Ambiente, 2017) for select Ocoña watershed analytes demonstrate the low concentration of solutes in the watershed (Table 1). The spread of metal(loid) values does not surpass drinking water and/or agricultural water quality standards except for As, which surpasses drinking water standards across all descriptive statistical values, and except for Fe and B which have maximum values that exceed the drinking water limit. It is interesting to note, that the Ocoña watershed displays much better water quality attributes compared to Peruvian water quality standards and neighboring watersheds, such as the Tambo watershed (Regis et al., 2022; Yang et al., 2023).

A principal component analysis (PCA) on 17 variables shows the top five principal components represent more than 80% of data variance (Table 2). However, Principal Component 1 and Principal Component 2 control most of the cumulative data variation (~60% total variance) in the Ocoña water dataset, demonstrated by the change in slope in a Scree Plot of cumulative variance (SI Fig. 1). Principal Component 1 (PC1) governs about 40% of variance and is controlled by Al–As–Ba–B–Ca–Li–Mg–Na along with pH. Principal Component 2 (PC2) governs about 20% of data variance and is controlled by Al–Cu–Fe–Mn and total suspended solids, with an inverse correlation with pH and As–Li.

Biplots show a strong separation of variable loading factors in Principal Component space, which can be grouped as hydrogeochemical signatures (see Table 2; Fig. 3). The two key hydrogeochemical signatures, highlighted by PCA, in the Ocoña watershed include: an Al–As–B–Ba–Ca–Li–Mg–Na metal(loid) association (PC1) and an Fe–Cu–Mn–Al metal association (PC2). Natural and anthropogenic controls on each hydrogeochemical signature is explored by grouping water data by: 1) elevation, 2) season, 3) rock type and 4) anthropogenic activities. Low elevation is defined by water samples collected at <1500 m.a.s.l., high elevation is categorized by water samples from >3000 m.a.s.l., and moderate elevation data is sampled between 1500–3000 m.a.s.l. elevation. Seasonal classification is categorized using precipitation and discharge data from Instituto Nacional de Recursos Naturales, 2007. Geology was grouped by Crystalline Rocks and Sedimentary-Volcanic

Table 1
Summary statistics of select variables in the Ocoña watershed compared with Peruvian water quality standards from Ministerio del Ambiente, 2017. Bold text highlights values that exceeds the drinking water quality standard.

Variable	Standards		Ocoña Water Data				
	Drinking[a]	Agriculture[b]	μ[c]	se[d]	max[e]	min[f]	med[g]
Ca (mg/L)	NA[h]	NA[h]	27.34	4.36	159.20	1.42	15.77
Na (mg/L)	NA[h]	NA[h]	30.81	3.77	152.39	2.07	26.48
Mg (mg/L)	NA[h]	NA[h]	5.06	0.74	28.33	0.29	3.37
Al (mg/L)	5	5	0.57	0.08	3.28	0.01	0.39
As (mg/L)	0.01	0.1	**0.04**	**0.02**	**0.97**	<0.01	**0.02**
B (mg/L)	2.4	1	0.69	0.19	**10.33**	<0.01	0.36
Ba (mg/L)	1	0.7	0.02	$2.20e^{-3}$	0.08	<0.01	0.02
Fe (mg/L)	1	5	0.46	0.07	**2.87**	0.02	0.30
Li (mg/L)	NA[h]	2.5	0.09	0.01	0.47	<0.01	0.07
Cu (mg/L)	2	0.2	<0.01	$6.27e^{-4}$	0.03	<0.01	<0.01
Mn (mg/L)	0.4	0.2	0.04	0.01	0.26	<0.01	0.02

[a] Surface water that is destined for drinking water with conventional treatment methods.
[b] Surface water for use in watering vegetables.
[c] Mean.
[d] Standard error.
[e] Maximum.
[f] Minimum.
[g] Median.
[h] Water standard is not specified.

Table 2
Principal component loading values and explained variance of the top principal components. Loading significance cut-off value is 0.24, representing a loading value where all variables contributed equally to the respective principal component. Significant principal component loadings are highlighted in bold text.

Variable	PC1[a]	PC2[b]	PC3[c]	PC4[d]	PC5[e]
Al (mg/L)	**0.27**	**0.28**	0.21	0.00	0.09
As (mg/L)	**0.26**	**−0.26**	0.17	0.03	0.16
Ba (mg/L)	**0.27**	0.19	**−0.23**	0.16	**−0.32**
B (mg/L)	**0.33**	−0.16	−0.04	**0.29**	0.05
Ca (mg/L)	**0.30**	0.02	**−0.31**	**−0.32**	0.00
Discharge (l/sec)	0.22	−0.13	**0.35**	0.05	0.11
Cu (mg/L)	0.14	**0.24**	**0.32**	−0.21	**−0.32**
Fe (mg/L)	0.05	**0.45**	**0.32**	−0.17	0.02
Li (mg/L)	**0.27**	**−0.30**	**0.24**	−0.02	0.19
Mg (mg/L)	**0.29**	−0.02	**−0.31**	**−0.36**	−0.10
Mn (mg/L)	0.21	**0.35**	0.03	**−0.29**	0.10
Na (mg/L)	**0.33**	−0.18	−0.17	−0.12	0.04
Total Suspended Solids (mg/L)	0.23	**0.36**	0.01	**0.38**	0.00
Temperature (°C)	0.19	0.14	−0.17	**0.58**	−0.11
Dissolved Oxygen (mg/L)	0.13	−0.23	**0.47**	0.04	−0.22
pH	**0.25**	**−0.25**	−0.04	−0.07	**−0.41**
Pb (mg/L)	0.18	0.09	−0.10	0.01	**0.67**
Explained Variance (%)	39.37	17.23	12.32	8.24	5.88

[a] Principal Component 1.
[b] Principal Component 2.
[c] Principal Component 3.
[d] Principal Component 4.
[e] Principal Component 5.

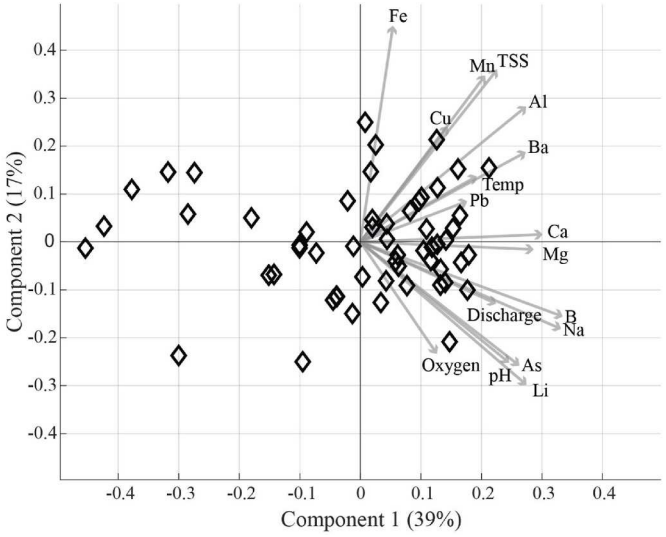

Fig. 3. Principal component analysis biplot for the first two principal components in Ocoña water data. Factor loadings are plotted for each variable. Key: TSS = Total Suspended Solids, Oxygen = Dissolved Oxygen, Temp = Temperature.

Rocks. Crystalline Rocks includes felsic to mafic intrusive rocks and metamorphic basement rocks. Sedimentary-Volcanic Rocks includes felsic to intermediate volcanic or volcaniclastic rocks, siliciclastic rocks, marl and limestone. Geology and anthropogenic activity are categorized based on maps presented in this study (Fig. 1). The correlation coefficient is calculated for each metal(loid) pair, comprising the hydrogeochemical signatures. Then, the average of correlation coefficient of pairs was calculated for each categorical group, identifying conditions where PC1 and PC2 metal(loids) have the strongest relationship (Fig. 4).

4.1.1. The Geothermal Association

Principal Component 1 metal(loids) show the strongest relationship with one another during both flood and dry seasons, at high elevation, and with sedimentary-volcanic rocks in mining-dominated and agriculture-mining-dominated areas (Fig. 4A). High elevations and a dominance of sedimentary-volcanic rocks are features of the northern part of the Ocoña watershed headwaters (see Fig. 1). This indicates that increasing PC1 metal(loid) (Al–As–B–Ba–Ca–Li–Mg–Na) concentrations, and increasing pH, are associated with the northern part of the Ocoña, where the predominant deposit types being mined are epithermal Au–Ag deposits (see Fig. 1B). Arsenic is a typical component of high-sulfidation epithermal deposits and found in abundant Cu–As sulfosalts (Plumlee et al., 1999) which matches mineralogical characteristics at the Selene deposit (Sucapuca, 2019) located north of the Ocoña watershed (Fig. 2). However, rock drainage from this deposit type tends to be acidic due to the presence of sulfosalts and sulfides (Plumlee et al., 1999), which is contrary to the positive metal(loid) relationship with pH in PC1 (Table 2). Moreover, typical drainage water chemistry from high sulfidation epithermal deposits often include other base metals like Fe and Cu in solution (Plumlee et al., 1999), which do not form part of the PC1

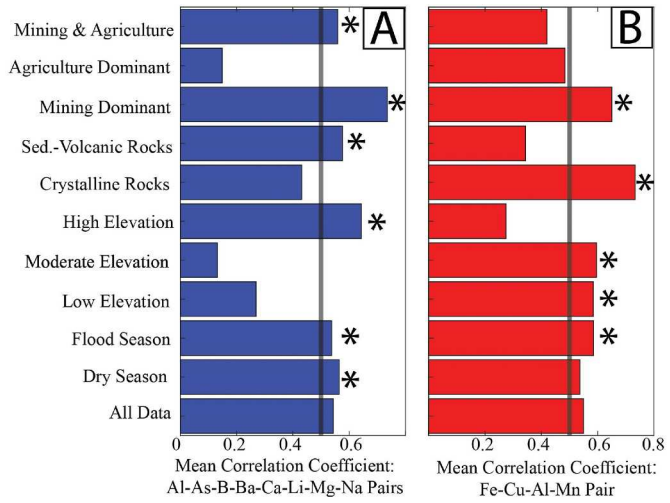

Fig. 4. A) Horizontal bar graphs of average correlation coefficient of metal (loid) pairs in PC1. B) Horizontal bar graphs of average correlation coefficient of metal pairs in PC2. The vertical line represents an average correlation coefficient (r) value of 0.5. Average r values are considered to represent a strong metal(loid) association if average r > 0.5 and if average r values of a data group is ≥ the average r value calculated using all data. Strong average r values are highlighted by an asterisk (*).

hydrogeochemical signature. Alternatively, this hydrogeochemical signature shares compositional similarities to solutes in geothermal hot spring and geyser waters in the Ocoña and neighboring watersheds. For example, As is found in high concentrations in the Ocoña watershed near hot springs (see Ccanccapa-Cartagena et al., 2021). Ciesielczuk et al. (2013) and Carrasco et al. (2021) documented elevated Li, B and Na in the neighboring Camaná watershed, suggesting solutes are sourced from nearby hot springs. In the Chili watershed, volcanic rocks are presented to be the source for Al, As, and B contamination (e.g. Autoridad Nacional del Agua, 2011; 2012, 2013b, 2014b). Additionally, in the neighboring Tambo watershed, Mg and Ca was documented in samples proximal to the Ubinas volcano (Autoridad Nacional del Agua 2015b, 2015c). Ultimately, this part of the Ocoña basin is a component of the *Eje Volcanico Sur* geothermal field (Vargas and Cruz, 2010), with over 150 hot springs having been mapped in the northern section of the Ocoña (Hanco Mamani, 2010). Due to these lines of evidence, the PC1 hydrogeochemical signature is characterized as a Geothermal Association.

4.1.2. The Acid Mine Drainage Association

Principal Component 2 metals show the strongest relationship with one another during the flood season, in low to moderate elevations, and where crystalline rocks and mining activity are prevalent (Fig. 4B). Moderate to low elevations and crystalline rocks are features reflective of the semi-arid, desert-like, southern part of the Ocoña where rivers drain to reach the Pacific Ocean (see Fig. 1). This indicates that increases in Fe–Cu–Mn–Al concentrations, increasing Total Suspended Solids, and decreasing pH are associated with the southern part of the Ocoña, where the dominant deposit types being mined are intrusion-related gold deposits and porphyry Cu–Mo deposits (see Fig. 1B). Principal Component 2 metals are common in porphyry and intrusion-related deposits, particularly found in pyrite and chalcopyrite (Fe and Cu) or silicates (Al) in alteration or hostrock mineral assemblages (intrusion-related deposits, see Crespo et al., 2020; Alfonso et al., 2019; Palacios et al., 2014; Palacios et al., 2011; porphyry Cu–Mo deposits, see Quang et al., 2003; Santos et al., 2019; Ye et al., 2022). Moreover, published literature supports a mining source for this hydrogeochemical signature as Fe, Mn and Al are common solutes associated with acid mine drainage (Plumlee et al., 1999; The International Network for Acid Prevention, 2009; Lee et al., 2002). In fact, a case study in Puerto Rico documents surface waters downstream from unmined porphyry copper deposits with elevated sulfate, Al, Cu, Fe and Zn (Berger et al., 2008). Based on the aforementioned observations, PC2 metals are likely sourced from acid mine drainage generated from intrusion-related and porphyry deposits in the southern Ocoña, leading to classification of this hydrogeochemical signature as an Acid Mine Drainage Association.

4.2. Concentration-discharge relationships

Concentration-discharge plots show hydrologic influences on the Geothermal Association and the Acid Mine Drainage Association, as a function of 1) elevation, 2) season, 3) rock type and 4) anthropogenic activities (SI Fig. 2). Flushing is the dominant CQ behavior exhibited by solutes in both the Geothermal and Acid Mine Drainage Associations (see SI Fig. 2). However, there are strong changes in CQ behavior when data are grouped by elevation and anthropogenic activity (Fig. 5; SI Fig. 2).

At high elevation, flushing is observed for most solutes in the Geothermal and Acid Mine Drainage Associations. However, progressive decreases in elevation show increasingly more non-systematic behavior and stronger flushing behavior, with increases in the coefficient of variance for solute concentration (Fig. 5). Additionally, dilution behavior becomes exhibited by more solutes at moderate elevations. The elevation-dependent shift to more non-systematic, and stronger flushing CQ behavior toward lower elevations, is likely reflecting the gaining flow nature of the river with decreasing elevation. Flushing processes are stronger and more efficient at lower elevations where a gaining stream experiences greater discharge. Furthermore, greater flushing could create more concentration data variability as increasing concentrations would be sensitive to high-discharge events, explaining the shift to more non-systematic behavior.

Anthropogenic influences on CQ behavior are more apparent with a shift from dominantly flushing behavior in mining-dominated regions to more dilution when agriculture is present (Fig. 5). Changes in CQ behavior, based on dominant anthropogenic activity, shows a control on metal(loid) mobility based on predominant land use (Fig. 5). When mining activity is dominant, flushing is the main CQ behavior, suggesting local storage of metal(loids) until high river flows incorporate these solutes into the rivers. However, when agriculture is a dominant anthropogenic activity, dilution becomes the main CQ behavior for metal(loid)s in the Geothermal Association. The shift from flushing to dilution in Geothermal Association metal(loid)s may be due to the introduction of nutrients, dissolved organic carbon (DOC), and solid organic matter from agriculture, typical components of agricultural soils (e.g. Royer and David, 2005). Evidence for contributions from agricultural soils includes elevated nutrient concentrations in streams where land is used for agriculture in the Ocoña watershed (SI Table 4). Agricultural soil components could be forming favorable aqueous complexes with some metals or inhibit the adsorption of Geothermal Association metal(loid)s. For example, the adsorption of arsenic has been shown to decrease in the presence of DOC (Grafe et al., 2001). Moreover, dissolved organic matter has been shown to reduce mobility of metals like Fe and Al through precipitation of organo-metal complexes and/or adsorption processes (Jansen et al., 2005), which would encourage storage on land soils. Storage of Fe and Al on soil would explain why Acid Mine Drainage Association metals retain flushing CQ behavior when agriculture is present alongside mining (Fig. 5). Conversely, Geothermal Association metal(loids) have increased mobility in the presence of agricultural soil components (nutrients, dissolved organic carbon (DOC), and solid organic matter), explaining the shift to dilution behavior (Fig. 5) when these components are incorporated into river water. Geothermal Association metal(loid) concentrations are greater when agriculture is a dominant anthropogenic activity (see SI Table 4), substantiating increased mobility of these variables.

Flushing is the main CQ behavior where the Geothermal Association (PC1) is principally expressed, specifically the dry season, at high

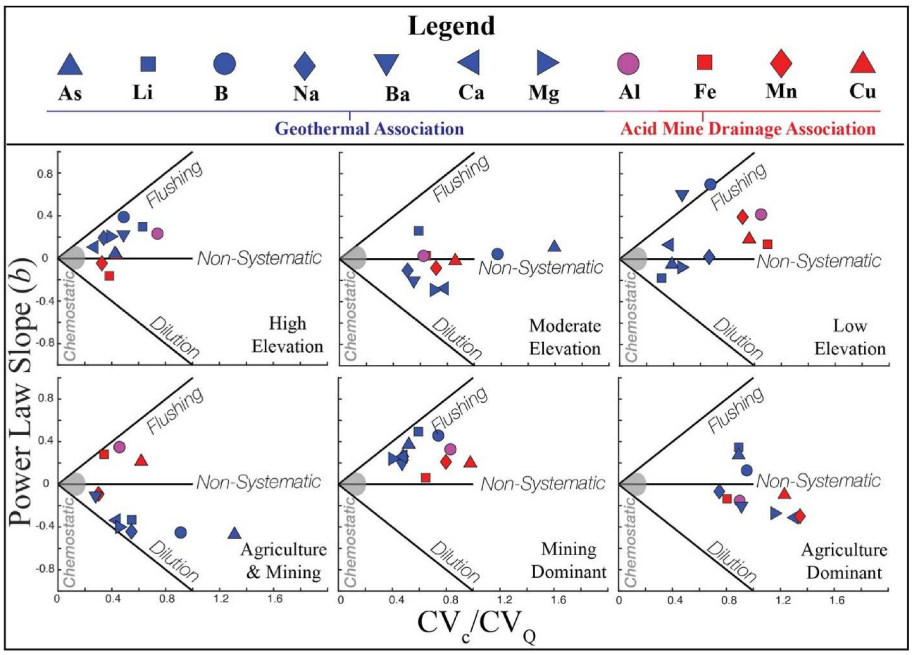

Fig. 5. Concentration-discharge plots of solutes in both hydrogeochemical signatures, grouped by elevation and anthropogenic activity. Plots are modelled after methods presented in Musolff et al. (2015).

elevation, and where sedimentary-volcanic rocks are dominant. This behavior suggests storage of Al–As–B–Ba–Ca–Li–Mg–Na in surrounding land (e.g. in soils and on plants) which would be flushed in high-precipitation events. Storage of solutes and flushing of readily-soluble precipitants from geothermal activity was reported from the neighboring Camaná watershed, at the Pinchollo geyser (Ciesielczuk et al., 2013). Flushing is also the main CQ behavior where the Acid Mine Drainage Association (PC2) is predominantly expressed, specifically in the flood season, at low to moderate elevations, and where crystalline rocks and mining activity are prevalent. Similar to the Geothermal Association, the Acid Mine Drainage Association metals are controlled by local storage of solutes and subsequent dissolution of soluble precipitants. Metals in acid drainage can be stored locally as secondary minerals such as sulfate slats including gypsum, jarosite, chalcanthite, brochantite, goslarite and pickeringite (Plumlee and Nash, 1995). These minerals often form coatings on surfaces during evaporation of acid drainage in the dry season, which are rapidly dissolved and contributed to local river water during high rain or snowmelt events (Plumlee and Nash, 1995). Expression of the Acid Mine Drainage Association in the flood season (see Fig. 4B) indicates a seasonal control on Fe–Cu–Mn–Al contribution through flushing. In arid climates, like the southern part of the Ocoña watershed, accumulation of secondary minerals, as opposed to acid mine drainage development, is typical and leads to minimal release of metals in dry seasons (Plumlee and Nash, 1995; The International Network for Acid Prevention, 2009). However, high precipitation events, mainly taking place in the flood season, cause immediate environmental threats to nearby surface water by dissolution and incorporation of salts into river water (Plumlee and Nash, 1995).

4.3. Geochemical processes in the southern Ocoña

Geochemical modeling explains the inverse relationship between metals and pH in the Acid Mine Drainage Association (PC1; Table 2). Eh-pH diagrams show pH-controlled precipitation of Fe–Cu–Mn–Al minerals and phases, emphasizing that increasing pH values will result in decreasing metal concentrations in solution (Fig. 6). Input conditions for Eh-pH plots used Ocoña water data from low to moderate elevations, where the Acid Mine Drainage Association is principally expressed (see Fig. 4B). Eh-pH diagrams show precipitation of iron hydroxide, copper ferrite, pyrolusite and gibbsite as low pH conditions are neutralized (Fig. 6).

Ocoña water data plotted on an Eh-pH plot (Fig. 6) show a reaction pathway trend going from low pH conditions, typical of acid mine drainage, evolving to near-neutral to basic conditions seen at the Ocoña. Proposed reaction pathways predict the following pH-controlled precipitation mechanisms for each of the Acid Mine Drainage Association metals:

$$\text{Iron: } Fe_2(OH)_2^{4+} + 4H_2O \Leftrightarrow 2Fe(OH)_3 + 4H^+ \quad (2)$$

$$\text{Aluminum: } Al^{3+} + 3H_2O \Leftrightarrow \text{Gibbsite} + 3H^+ \quad (3)$$

$$\text{Manganese: } Mn^{2+} + 2H_2O \Leftrightarrow \text{Pyrolusite} + 4H^+ + 2e^- \quad (4)$$

$$\text{Copper: } Cu^{2+} + H_2O \Leftrightarrow \text{Tenorite} + 2H^+ \quad (5)$$

$$\text{Copper with Iron: } Cu^{2+} + 4H_2O + 2Fe^{++} \Leftrightarrow \text{Ferrite-Cu} + 8H^+ + 2e^- \quad (6)$$

Geochemical modeling shows an increasing pH thermodynamically favors precipitation of all four Acid Mine Drainage Association metals. However, individual correlation coefficient pairs of each metal with pH shows that Fe has the strongest inverse relationship with pH. Conversely, Cu, Mn and Al have insignificant, weak positive correlation coefficient values when paired with pH. This suggests Fe is the main metal precipitating out of solution during increasing pH, forming $Fe(OH)_3$ (see Fig. 6). Copper, Mn and Al are removed from solution due to processes that are not influenced by pH changes, likely reflective of sorption. Precipitants like Fe-oxyhydroxides have been known to serve as a surface for sorption of other metals (e.g. Johnson, 1986; Lee et al., 2002; Munk et al., 2002; Sánchez-España et al., 2006; Carrero et al., 2015), corroborating sorption of Cu, Al and Mn onto freshly-precipitated $Fe(OH)_3$ as a likely mechanism. Therefore, it is suggested here that precipitation of Fe due to increases in pH is the leading mechanism for removal of Acid Mine Drainage Association metals from river water. Other metal(loids), like As and Pb, have also been known to sorb onto recently-formed suspended Fe and Al precipitants (Plumlee, 1999). Sorption of As onto Fe precipitants could explain the inverse relationship of As with Acid Mine Drainage Association metals in PC2 (Table 2). Other toxic heavy metals and metalloids in river water (i.e. certain

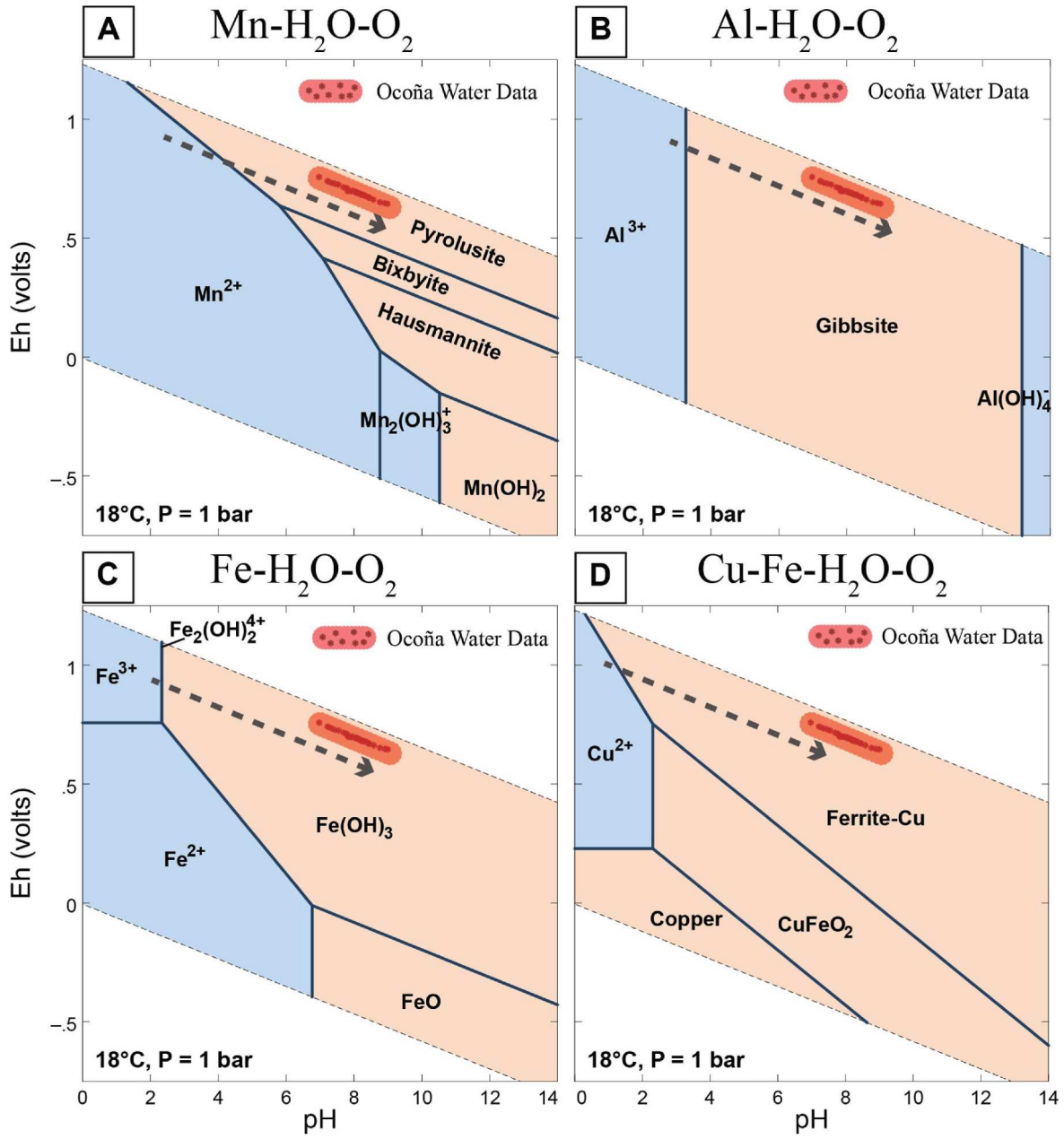

Fig. 6. Eh-pH diagrams for each metal in the Acid Mine Drainage Association (PC2). The red field represents the redox and pH conditions of Ocoña river water sampled. Pressure and temperature conditions used in the model reflect the water conditions in the Ocoña watershed where the Acid Mine Drainage Association is present. The arrow indicates the proposed reaction path for the systems (A) Mn–H_2O–O_2; (B) Al–H_2O–O_2; (C) Fe–H_2O–O_2; and (D) Cu–Fe–H_2O–O_2. Minerals and aqueous species considered for Fe diagrams are: Fe^{2+}, Fe^{3+}, $Fe(OH)_2$, $Fe(OH)_2^+$, $Fe(OH)_3$, $Fe(OH)_3^-$, $Fe(OH)_4^-$, $Fe_2(OH)_2^{4+}$, $Fe_3(OH)_4^{5+}$, $FeOH^+$, $FeOH^{2+}$, $Fe(OH)_2$(ppd), $Fe(OH)_3$(ppd) and FeO(c). Iron mineral phases that were suppressed were wustite, goethite, hematite, and magnetite to allow for amorphous solid phases to form over ordered mineral phases. Minerals and aqueous species considered for Al diagrams are: Al^{3+}, $Al(OH)_2^+$, $Al(OH)_3$, $Al(OH)_4^-$, $Al_{13}O_4(OH)_{24}^{7+}$, $Al_2(OH)_2^{4+}$, $Al_3(OH)_4^{5+}$, $AlOH^{2+}$, boehmite, corundum, diaspore and gibbsite. Minerals and aqueous species considered for Mn diagram species are: Mn^{2+}, MnO_4^-, MnO_4^{2-}, $Mn(OH)_2$, $Mn(OH)_3^-$, $Mn(OH)_4^{2-}$, $Mn_2(OH)_3^+$, Mn_2OH^{3+}, $MnOH^+$, birnessite, bixbyite, hausmannite, manganite, manganosite, $Mn(OH)_2$(am), $Mn(OH)_3$(c), pyrolusite and todorokite. Minerals and aqueous species considered for Cu diagram species are: Cu^+, Cu^{2+}, $CuOH^+$, native copper, cuprite and tenorite. However, Cu diagram species in the presence of Fe includes $CuFeO_2$(c) and Ferrite-Cu as phases.

Geothermal Association solutes) can potentially sorb onto Fe-precipitants as well. Metal oxides or Fe-oxide floc have been suggested as useful treatment methods to address As and B contamination from geothermal solutions (As; Webster and Nordstrom, 2003; B; Mott et al., 2022). Webster and Nordstrom (2003) note that the removal of geothermal contaminants, such as As, is rarely from a point-source location and is rather widespread due to the complex plumbing of most geothermal systems. Therefore, the importance of conventional water treatment plants for As removal is highlighted for geothermal-sourced contamination (Webster and Nordstrom, 2003).

Sorption of Cu on Fe-precipitants does not appear to be as effective in removing Cu from solution in the flood season. A Kruskal-Wallis Statistical Test ($p > 0.40$) on Fe, Mn and Al concentrations between the dry season and flood season shows there is no statistical difference between the two seasons. Copper, however, has a higher maximum concentration in the flood season and a Kruskal-Wallis Statistical Test ($p = 0.13$) suggests a probable statistical difference in the processes controlling Cu behavior between the dry and flood seasons. Sorption of Cu onto oxides

and hydroxides is a strong mechanism for regulating Cu concentrations in water, particularly at near-neutral pH conditions due to increased sorption efficiency with increasing pH (Johnson, 1986; Smith, 1999; Pokrovsky et al., 2008). Consequently, strong sorption of Cu onto Fe-hydroxide is expected in the flood season of the Ocoña watershed where pH conditions are near-neutral (average Ocoña water pH ~ 8). Unexpected, less-effective sorption of Cu onto Fe-hydroxide in the Ocoña may be due to competing mechanisms that control Cu speciation in river water during the flood season, such as complexation with DOC incorporated during flushing events. At pH values that are closer to neutral, Cu complexation with DOC is a strong mechanism facilitating metal transport (pH = 6.6; Temminghoff et al., 1997; pH > 5.0; Strobel et al., 2001). Furthermore, Sunda and Hanson (1979) found that dissolved copper is predicted to mainly occur as organic complexes in rivers. Ultimately, the release of Cu at higher pH settings (pH > 5) is controlled by in-solution complexation by DOC (Strobel et al., 2001), which are the pH conditions in Ocoña river water. Increased complexation of Cu with DOC would result in greater stability of Cu in solution and therefore increased concentrations. However, experimental and calculated (biotic ligand model) water quality criteria (WQC) shows toxicity of Cu is reduced in water with higher DOC concentrations (Villavicencio et al., 2005). Furthermore, various studies have shown that natural organic matter in natural water reduces bioavailability of metals proportional to its concentration in water (Smith et al., 2015 and references therein). Greater DOC concentrations during the flood season is likely as these months would experience more flushing events, where water overflows onto surrounding land, incorporating not only stored metal-bearing solutes, but also other land components like organic-rich humus found in soils (e.g. Morel et al., 2009). Therefore, it is proposed that Cu complexation with ligands is competing with Cu-sorption onto Fe-hydroxide surfaces and is more pronounced in the flood season where flushing processes incorporate more DOC into the river. At Ocoña river water pH conditions (pH 8), Cu-DOC complexation prevails over Fe-DOC and Al-DOC complexation due to the reduced solubility of these metals with increasing pH (see Strobel et al., 2001), explaining the increase in Cu concentration in the flood season and not Fe and Al. Prior work in the neighboring Tambo watershed revealed no correlation between the Cu concentration and wet and dry seasons despite higher overall Cu concentrations (Yang et al., 2023). Nevertheless, the 0.03 mg/L maximum Cu concentrations documented in the Ocoña watershed do not reach the 0.20 mg/L irrigation water standard set by Peru (Ministerio del Ambiente, 2017) nor the ~0.04 mg/L WQC observed and calculated in high-DOC waters (experimentally observed WQC = 38.7 μg/L; Biotic Ligand Model calculated WQC = 35.3 μg/L; Villavicencio et al., 2005). However, the dissolved copper criterion maximum concentration reported for freshwater animals is ~0.002 mg/L (2.337 μg/L; U.S. Environmental Protection Agency, 2007) which is significantly lower than the 0.03 mg/L maximum Cu concentration observed in the Ocoña watershed during the flood season. Therefore, ecotoxicity of Cu may still be a concern in the Ocoña watershed.

4.4. Mineralogical controls on the Acid Mine Drainage Association

Results from mineralogical studies on the San Juan de Chorunga show evidence for mineralogical controls on the pH of river water in the southern part of the Ocoña watershed, where the Acid Mine Drainage Association is expressed. Deposit mineralogy is therefore a key component to acid-neutralization and subsequent Fe–Cu–Mn–Al removal from solution through precipitation and sorption.

Quantitative mineral modal abundances of veins and tailings from San Juan de Chorunga show the main minerals in the deposit type are quartz, calcite and pyrite (Fig. 7). However, there is mineralogical variability within the same mineral deposit, such as greater calcite abundances in deeper vein samples and greater pyrite abundances in samples collected at intermediate to greater depths (Fig. 7) which was noted in Crespo et al. (2020). Furthermore, near-surface veins samples

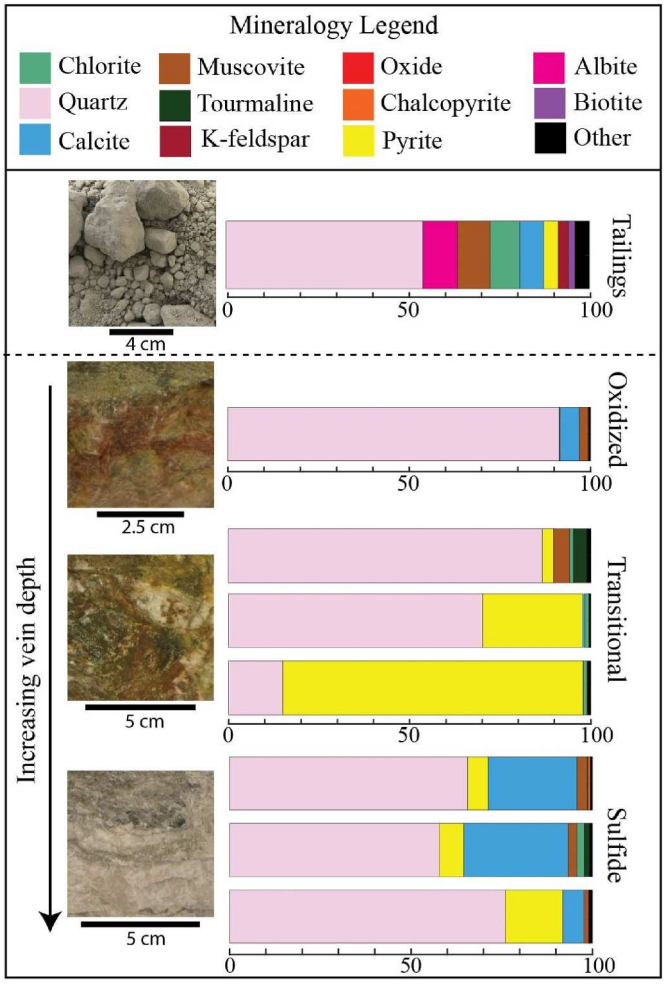

Fig. 7. Horizontal stacked bar plots of mineral modal abundance data in tailings and vein samples from San Juan de Chorunga analyzed using automated mineralogy. Photographs of samples show tailings texture and changes in vein expression from near-surface to deeper portions of the mine.

contain Fe-oxides, Fe-oxyhydroxides, and supergene copper minerals in only minor to trace phases (Fig. 7), despite being observed in macroscopic and petrographic studies (Crespo et al., 2020). Tailings largely represents the mineralogy observed in ore veins except for albite, biotite and K-feldspar (Fig. 7). These minerals are dominant in the granodioritic-dioritic intrusive rock that hosts ore veins, which is likely contributing material during mineral processing. Furthermore, mineral processing preserves or concentrates gangue minerals including chlorite and calcite, which are capable of neutralizing low-pH conditions. Chlorite mineral modal abundance is 0.0%–2.2 % in vein samples and up to 8.2% in tailings. Chlorite has been shown to be capable of neutralizing acid (e.g. O'Neill et al., 2004; Yager et al., 2005; Bove et al., 2008; Yager, 2008) and is likely contributing to increasing pH where acid mine drainage is developed. Results from BSE imaging show mineral dissolution textures in chlorite, particularly where sulfide inclusions are present (Fig. 8A). Sulfide inclusions in chlorite show dissolution textures along surface and cleavage planes, however, chlorite preserves a stable form when lacking sulfide inclusions (Fig. 8B). This means chlorite is being dissolved and acts as a pH buffer, neutralizing the acidity generated by sulfide oxidation and is therefore helpful in acid neutralization on a local scale. Calcite also shows mineral dissolution textures (Fig. 8C and **D**) and is widely considered an effective mineral for neutralizing acid mine drainage (e.g. Maree and du Plessis, 1994; Plumlee and Nash, 1995; Galan et al., 1999). Although calcite and chlorite are essential to acid neutralization, pyrite is likely responsible for acid generating

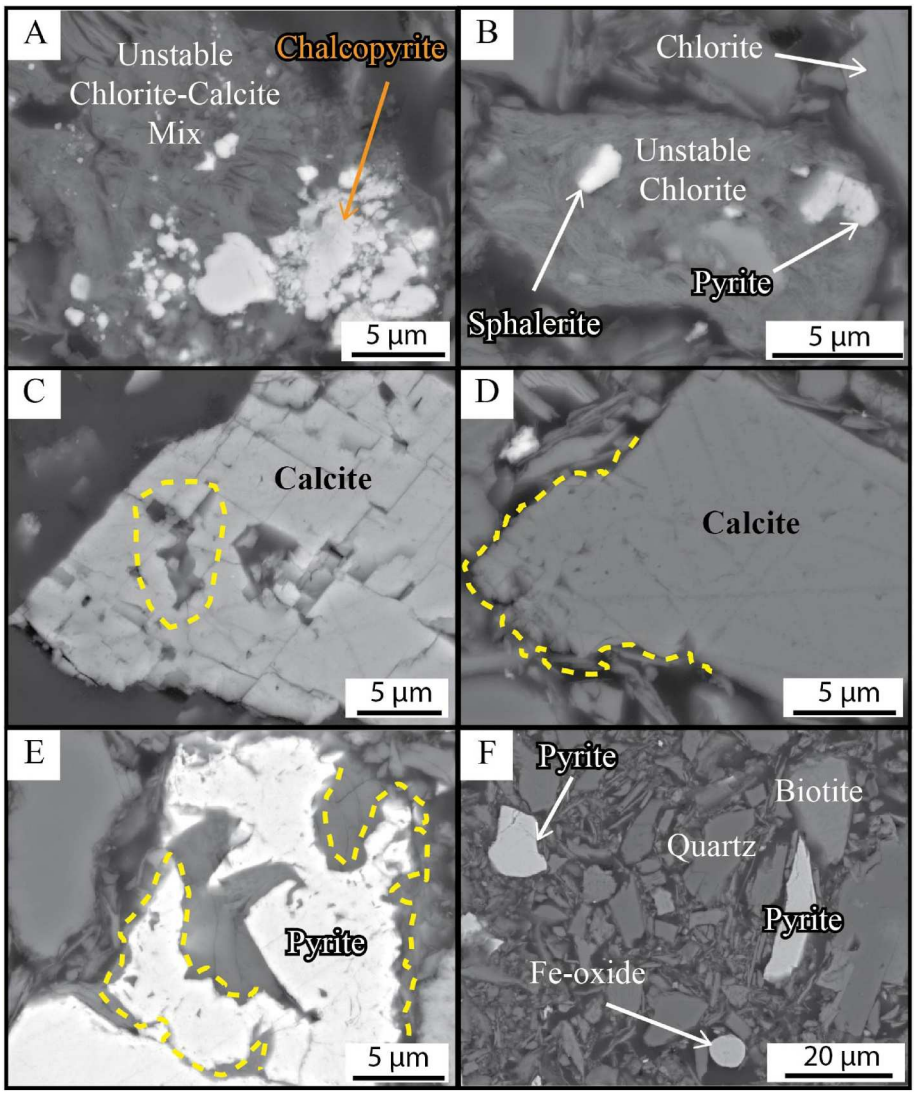

Fig. 8. Backscattered electron images of the mineralogy and mineralogical association of tailings samples from San Juan de Chorunga showing variable dissolution and reaction features. (A) Irregular chalcopyrite inclusions in unstable chlorite and calcite. (B) Sphalerite and pyrite inclusions in irregular, unstable chlorite. The top right features pristine chlorite, without sulfide inclusions. (C) Euhedral calcite showing excellent cleavage breakage. A section of the calcite crystal with irregular boundaries, contrasting cleavage, is highlighted in a dotted yellow line. (D) Euhedral calcite with soft edges highlighted in a yellow dashed line. (E) Fragmented euhedral pyrite with irregular grain boundaries highlighted by dashed yellow lines. (F) Mineral grains in tailings, showing pyrite, quartz and biotite as individual grains as a result of liberation during mineral processing.

processes in mineral deposits of the southern Ocoña. Pyrite is the dominant sulfide phase in intrusion-related deposits of the southern Ocoña (Fig. 7) which is a mineralogical characteristic responsible for acid mine drainage globally through oxidation processes (Nordstrom and Alpers, 1999; INAP, 2009; Nordstrom et al., 2015). Furthermore, pyrite dissolution textures are observed in tailings showing fragmented mineral grains and irregular grain boundaries (Fig. 8E), supporting interpretations that acid mine drainage is generated from pyrite oxidation.

Encapsulation and interlocking of sulfide phases like pyrite can have a significant impact on the dissolution of sulfides due to the lack of exposure to the environment that mineral-encasement provides. For example, in cases where sulfides are encapsulated by quartz or any other mineral phase that is chemically inert, the environmental effects of the sulfide phases may be lower (Davis et al., 1994; John and Leventhal, 1995). Mineral associations calculated in quantitative mineralogical analysis reveals pyrite is predominantly associated with quartz, calcite, and chlorite in Ocoña intrusion-related deposits. Encapsulation of pyrite by minerals that are non-reactive (quartz) or acid-neutralizing (calcite and chlorite; Fig. 8A and D) is expected to help by reducing acid generation in rocks being mined. However, most pyrite was effectively liberated during mineral processing, exposing mineral surfaces to oxidizing ambient surface conditions (Fig. 8F). Therefore, processed mineral deposits in the southern Ocoña and the resultant tailings are likely to generate acid mine drainage as pyrite is no longer encapsulated by non-reactive or acid-neutralizing minerals.

Detailed mineralogical studies on San Juan de Chorunga show acid-neutralizing minerals (i.e. calcite and chlorite; Fig. 8) are present in intrusion-related gold deposits in the southern Ocoña. These minerals are also present in porphyry Cu–Mo deposits, the other main deposit type found in the southern Ocoña. Calcite and chlorite are common propylitic alteration assemblages which typically exist as wide alteration halos in porphyry Cu–Mo deposits in Arequipa (Quang et al., 2003; Santos et al., 2019; Ye et al., 2022). Therefore, acid neutralizing processes described for Ocoña intrusion-related deposits are also expected at Ocoña porphyry Cu–Mo deposits due to a similar alteration and ore mineralogy. Processes where carbonate and propylitically-altered rocks neutralize acidic drainage has been documented at Red Mountain Pass, southwest Colorado, USA (Plumlee, 1999). Akin to the geochemical

processes proposed in this study (Fig. 6), at Red Mountain Pass, acid-neutralization by calcite- and chlorite-bearing rocks results in Fe-, Al- and Mn-rich colloids and particulates formation with subsequent metals sorption (Plumlee, 1999).

5. Conclusions

Past watershed-comparative studies focus on the region (Regis et al., 2022; Yang et al., 2023) and descriptive statistics explored within this study have demonstrated favorable water quality within the Ocoña watershed despite profuse mining activity. This is a result of the natural geochemical and seasonal processes taking place in the Ocoña watershed. The pH levels between the southern and northern segments of the Ocoña watershed differ slightly. The -log of average hydrogen ion concentrations [H^+] in the southern Ocoña is 8.2 (95% Confidence Interval (CI) from 8.1 to 8.4), and is 8.0 (95% CI from 7.9 to 8.1) in the northern Ocoña. The difference in pH may be explained by differing contaminant sources and differing host rock and deposit types, and concomitant alteration mineralogy assemblages across these two segments.

Association analysis reveals that acid mine drainage strongly contributes Fe, Cu, Mn and Al in the southern section of the Ocoña watershed. In this region, anthropogenic contributions likely play a strong role due to mining of intrusion-related and porphyry Cu–Mo deposits in addition to natural oxidation associated with weathering. Despite these metal contributions, there is little degradation of overall water quality with respect to toxic metal(loid)s. A potential explanation is acid neutralization through reaction and dissolution of calcite and chlorite in veins and propylitic alteration assemblages. Acid neutralization in turn induces pH-controlled precipitation of Fe which can serve as a substrate for the subsequent sorption of potentially more toxic metals such as copper onto amorphous Fe-oxyhydroxides. Although Fe, Cu, Mn and Al concentrations are largely buffered by precipitation and sorption processes, contamination of these metals is most pronounced during high flows in the wet season during which time, metals are flushed from local storage into surrounding floodplains. In this window, Fe values exceed drinking water limits and maximum Cu values exceed ecotoxicological standards. However, increased DOC could reduce the toxic effects of Cu, as DOC serves as a ligand to the metal concurrently reducing ecotoxicity (Villavicencio et al., 2005).

In the northern Ocoña, association analyses revealed that Al, As, B, Ba, Ca, Li, Mg and Na are primarily introduced to river water through geothermal activity and hot springs. This hydrogeochemical signature is most pronounced where mining, with or without agriculture, is present. Metal(loids) are flushed into the river during high-discharge events after geothermal precipitants have been stored in surrounding floodplains. However, the presence of agricultural activity increases the mobility of these metal(loid)s, evidenced by CQ-relationships and by the greater metal(loid) concentrations in solution where agriculture is dominant, compared to mining-dominated regions. Boron and As may be of concern within this northern Ocoña region as descriptive statistics show concentrations of these metalloids exceed drinking water limits. Products of Fe-precipitation ($Fe(OH)_3$), formed during neutralization of acid mine drainage in the southern Ocoña, could play a role to help mitigate the further transport of B and As from the northern Ocoña as metal oxides and Fe-oxide floc have been noted as useful treatment methods for As and B (As; Webster and Nordstrom, 2003; B; Mott et al., 2022). However, conventional water treatment plants are still considered to be the more effective solution to remove geothermal-sourced contaminants (Webster and Nordstrom, 2003).

This study identifies factors responsible for metal contamination in the Ocoña river. Results demonstrate the importance of deposit mineralogy and high-precipitation events on contamination. Understanding the impacts of mineral deposits and concomitant water-rock interactions will allow for efficient mitigation strategies to minimize the degradation of the water quality in semi-arid regions such as the Ocoña that may further harbor conflict and concern over water resources. The implementation of strategies that control the introduction of constituents such as boron, arsenic and copper, which can impair agricultural productivity, ecosystem and/or human health, is also essential to maintaining the health and wellbeing of populations that rely on the local water supplies. The workflow presented in this study may have a global application to establish source hydrogeochemical fingerprints and identify major contributing factors. This in turn can be applied to inform management strategies and may further provide a tool that helps predict the impact of current and future anthropogenic activities on surface water quality.

CRediT authorship contribution statement

Isaac J.P. Simon: Writing – review & editing, Writing – original draft, Investigation, Formal analysis, Data curation. **Katharina Pfaff:** Writing – review & editing, Writing – original draft, Supervision, Resources, Methodology, Funding acquisition, Conceptualization. **Alexis Navarre-Sitchler:** Writing – review & editing, Writing – original draft, Supervision, Methodology. **Jorge Crespo:** Writing – review & editing, Resources, Conceptualization. **Elizabeth Holley:** Writing – review & editing, Project administration, Funding acquisition, Conceptualization. **Gary Vanzin:** Writing – review & editing, Validation, Resources, Formal analysis, Data curation. **Madeleine N. Guillen Gomez:** Writing – review & editing, Project administration, Funding acquisition, Conceptualization. **Sergio Ticona-Corrales:** Writing – review & editing, Resources, Funding acquisition, Conceptualization. **Jonathan O. Sharp:** Writing – review & editing, Validation, Methodology, Funding acquisition.

Declaration of competing interest

The authors declare that they have no known competing financial interests or personal relationships that could have appeared to influence the work reported in this paper.

Data availability

Data are available in Supplementary Information

Acknowledgements

The Center for Mining Sustainability, a collaboration between Universidad Nacional San Agustín of Arequipa in Perú and the Colorado School of Mines provided funding of this project. Part of this research was supported by the National Science Foundation through the Center to Advance the Science of Exploration to Reclamation in Mining under award numbers 2310920 and 2310948. Professor Ahmadreza Hedayat and his research group at the Colorado School of Mines generously supplied San Juan de Chorunga tailings sample material for this study. Roberto Huamani provided detailed insights on the tailings pile sampling approach. Dr. Thomas Monecke provided insightful discussions which improved our research approach. Andy Yahya Al Hakim and Connor Newman provided exceptional insights and recommendations that improved this manuscript.

Appendix B. Supplementary data

Supplementary data to this article can be found online at https://doi.org/10.1016/j.apgeochem.2024.106028.

References

Abraham, M.R., Susan, T.B., 2017. Water contamination with heavy metals and trace elements from Kilembe copper mine and tailing sites in Western Uganda; implications for domestic water quality. Chemosphere 169, 218–287.

Acosta, J., Quispe, J., Rivera, R., Valencia, M., Chirif, H., Huanacuni, D., Rodríguez, I., Villarreal, E., Paico, D., Santisteban, A., 2010. Mapa Metalogenético del Oro en Perú. Reporte de Instituto Geológico Minero y Metalúrgico, p. 15.

Adjei, R., Stevens, J.R., 2022. Handling non-detects with imputation in a nested deisgn: a simulation study. In: Conference on Applied Statistics in Agriculture and Natural Resources 2022. https://doi.org/10.26077/693e-25f0.
Alfonso, P., Anticoi, H., Yubero, T., Bascompta, M., Henao, L., Garcia-Valles, M., Palacios, S., Yañez, J., 2019. The importance of mineralogical knowledge in the sustainability of artisanal gold mining: a mid-south Peru case. Minerals 9 (6), 345.
Armienta, M.A., Talavera, O., Villaseñor, G., Espinosa, E., Pérez-Martínez, I., Cruz, O., Ceniceros, N., Aguayo, A., 2004. Environmental behaviour of metals from tailings in shallow rivers: taxco, central Mexico. B. Appl. Earth Sci. 113 (1), 76–82.
Autoridad Nacional del Agua, 2011. Resultados del segundo monitoreo de la calidad del agua en la Cuenca Chili – Arequipa 2011, p. 83. Informe Técnico No. 108-2011-ANA-AAA/C-O/SDCPRH/MPPC-GBR.
Autoridad Nacional del Agua, 2012. Primer monitoreo de calidad de aguas del Rio Chili-Arequipa del 20 al 27 de Agosto del 2011, p. 222. Informe Técnico No. 002-2012-ANA/PMGRH-GBR-AAA/C-O/SDGCRH/MPPC.
Autoridad Nacional del Agua (ANA), 2013a. Informe del Primer Monitoreo de Calidad de Agua Superficial en la Cuenca del Rio Ocoña, Abril. Informe Técnico No. 006-2013-ANA-AA CO-SDGCRH/JLFZ 107.
Autoridad Nacional del Agua, 2013b. Informe de resultados del primer monitoreo participativo de la calidad del agua en la Cuenca Quilca Chili, realizado del 21 de enero al 01 de febrero del 2013, p. 273. Informe Técnico No. 001-2013-PMGRH-CUENCA CHILI/LGEQ.
Autoridad Nacional del Agua (ANA), 2014a. Informe del Segundo Monitoreo Participativo de Calidad de Agua Superficial en la Cuenca del Rio Ocoña, Julio. Informe Técnico No. 005-2014-ANA-AAA CO-SDGCRH/JLFZ 128.
Autoridad Nacional del Agua, 2014b. Informe Técnico del primer monitoreo participativo de la calidad del agua superficial en la Cuenca Quilca-Chili periodo 2014. Informe Técnico No. 001-2014-PMGRH-CUENCA CHILI/LGEQ 193.
Autoridad Nacional del Agua (ANA), 2015a. Informe del Tercer Monitoreo Participativo de Calidad de Agua Superficial en la Cuenca del Rio Ocoña, Mayo. Informe Técnico No. 020-2015-ANA-AAA CO-ALA-OP/FGA 136.
Autoridad Nacional del Agua, 2015b. Monitoreo de calidad de agua en el sector de Ubinas. Informe Técnico No. 004-2015-ANA-AAA.CO-ALA.TAT/VCA 33.
Autoridad Nacional del Agua, 2015c. Monitoreo de calidad de agua en el sector Ubinas. Informe Técnico No. 037-2014-ANA-AAA.CO-ALA.TAT/VCA 19.
Bantis, L., 2024. Fit distributions to censored data. MATLAB central file exchange. https://www.mathworks.com/matlabcentral/fileexchange/38226-fit-distributions-to-censored-data. (Accessed 1 February 2024).
Berger, B.R., Ayuso, R.A., Wynn, J.C., Seal, R.R., 2008. Preliminary Model of Porphyry Copper Deposits, vols. 2008–1321. U.S. Geological Survey Open-File Report, p. 55.
Bethke, C.M., 2007. Geochemical and Biogeochemical Reaction Modeling. Cambridge University Pres, p. 564.
Boekhout, F., Sempere, T., Spikings, R., Schaltegger, U., 2013. Late Paleozoic to Jurassic chronostratigraphy of coastal southern Peru: temporal evolution of sedimentation along an active margin. J. S. Am. Earth Sci. 47, 179–200.
Bove, D.J., Lowers, H.A., Plumlee, G.S., Verplanck, P.L., 2008. Chapter C: in-situ acid weathering reactions in areas affected by large-scale and pervasive hydrothermal alteration in the southern rocky Mountains. In: Verplanck, P.L. (Ed.), Understanding Contaminants Associated with Mineral Deposits, vol. 1328. U.S. Geological Survey Circular, pp. 14–17.
Brain, K.A., 2017. The impacts of mining on livelihoods in the Andes: a critical overview. Extr. Ind. Soc. 4, 410–418.
Carrasco, M., Renou, F., Peña, F., Acosta, A., Olarte, Y., Sanchez, M., Cotrina, G., Vargas, V., Snatos, B., 2021. Estudio hidrogeológico de la Cuenca del río Camaná-Majes-Colca. Instituto Geológico Minero y Metalúrgico Boletín Serie H: Hidrogeologia 8, 295.
Carrero, S., Perez-Lopez, R., Fernandez-Martinez, A., Cruz-Hernandez, P., Ayora, C., Poulain, A., 2015. The potential role of aluminium hydrooxysulphates in the removal of contaminants in acid rock drainage. Chem. Geol. 417, 414–423.
Ccanccapa-Cartagena, A., Paredes, B., Vera, C., Chavez-Gonzalez, F.D., Olson, E.J., Welp, L.R., Zyaykina, N.N., Filley, T., Warsinger, D.M., Jafvert, C.D., 2021. Occurrence of probabilistic health risk assessment (PRA) of dissolved metals in surface water sources in Southern Peru. Environ. Adv. 5, 100102.
Ciesielczuk, J., Zaba, J., Bzowska, G., Gaidzik, K., Glogowka, M., 2013. Sulphate efflorescences at the geyser near Pinchollo, southern Peru. J. S. Am. Earth Sci. 42, 186–193.
Concas, A., Ardau, C., Cristini, A., Zuddas, P., Cao, G., 2006. Mobility of heavy metals from tailings to stream waters in a mining activity contaminated site. Chemosphere 63 (2), 244–253.
Costa, M., Alfonso, P., Palacios, S., 2009. Proceso de tratamiento para la recuperación de oro en el asentamiento minero artesanal de Misky. Segundo Congreso Internacional sobre Geología y Minería en la Ordenación del Territorio y en el Desarrollo. Utrillas, Spain.
Crespo, J., Holley, E., Pfaff, K., Guillen, M., Huamani, R., 2020. Ore mineralogy, trace element geochemistry and geochronological constraints at the Mollehuaca and San Juan de Chorunga Au-Ag Vein deposits in the Nazca-Ocoña Metallogenic Belt, Arequipa, Peru. Minerals 10, 1112.
Cuadros, M.F.B., 2022. Bridge and boundary: the maritime connections of colonial Arequipa, Peru. Int. J. Hist. Archaeol. 26, 291–315. https://doi.org/10.1007/s10761-021-00599-3.
Davis, A., Ruby, M.V., Bergstrom, P.D., 1994. Factors controlling lead bioavailability in the Butte mining district, Montana, USA. Environ. Geochem. Health 3/4, 147–157.
Dietrich, A., Nelson, E.P., Palacios, C., Layer, P.W., 2005. Geology of the Explorador Ag-Au vein system and Selene mining district, Apurimac, Peru. In: Rhoden, H.N., Steininger, R.C., Vikre, P.G. (Eds.), Window to the World. Geological Society of Nevada 2005 Symposium Proceedings, pp. 741–756. Reno, Nevada.
Galan, E., Carretero, M.I., Fernandez-Caliani, J.C., 1999. Effects of acid rock drainage on clay minerals suspended in the Tinto River (Río Tinto, Spain). An experimental approach. Clay Miner. 34, 99–108.
Godsey, S.E., Kirchner, J.W., Clow, D.W., 2009. Concentration-discharge relationships reflect chemostatic characteristics of US catchments. Hydrol. Process. 23, 1844–1864.
Grafe, M., Eick, M.J., Grossl, P.R., 2001. Adsorption of arsenate (V) and arsenite (III) on geothite in the presence and absence of dissolved organic carbon. Soil Sci. Soc. Am. J. 65, 1680–1687.
Hanco Mamani, W.M., 2010. GEOCATMIN: Sistema de información geológico y catastral minero. Sociedad Geológica del Perú, XV Congreso Peruano de Geología, Cusco, Pub, vol. 9. Esp, pp. 1319–1323.
Helsel, D.R., 2005. More than obvious: better methods for interpreting nondetect data. Environ. Sci. Technol. 39 (20), 419A–423A. https://doi.org/10.1021/es053368a.
Hoagland, B., Navarre-Sitchler, A., Cowie, R., Singha, K., 2020. Groundwater-stream connectivity mediates metal(loid) geochemistry in the hyporheic zone of streams impacted by historic mining and acid rock drainage. Front. Water 2, 600409. https://doi.org/10.3389/frwa.2020.600409.
Instituto Nacional de Recursos Naturales, 2007. Evaluación de recursos hídricos de la Cuenca del río Ocoña: Estudio hidrológico. Ministerio de Agricultura, Instituto Nacional de Recursos Naturales Intendencia de Recursos Hídricos Informe Final 1, 163. https://hdl.handle.net/20.500.12543/3886.
Jansen, B., Nierop, K.G.J., Verstraten, J.M., 2005. Mechanisms controlling the mobility of dissolved organic matter, aluminum and iron in podzol B horizons. Eur. J. Soil Sci. 56, 537–550.
John, D.A., Leventhal, J.S., 1995. Bioavailability of metals. In: du Bray, E.A. (Ed.), Preliminary Compilation of Descriptive Geoenvironmental Mineral Deposit Models, vols. 95–831. U.S. Geological Survey Open-File Report, pp. 10–18.
Johnson, C.A., 1986. The regulation of trace element concentrations in river and estuarine waters contaminated with acid rock drainage: the adsorption of Cu and Zn on amorphous Fe oxyhydroxides. Geochem. Cosmochim. Acta 50, 2433–2438.
Lasage, R., Ward, P.J., Belinfante, T., Singh, M., de Moel, H., 2011. Impact of Climate Change of Modelled Runoff of the Ocoña River in Peru. Institute for Environmental Studies, p. 29. Report R-11/09.
Lee, G., Bigham, J.M., Faure, G., 2002. Removal of trace metals by coprecipitation with Fe, Al and Mn from natural waters contaminated with acid rock drainage in the Ducktown Mining District, Tennessee. Appl. Geochem. 17 (5), 569–581.
Lewis, T.B., Garcia-Chevesich, P.A., Wildeman, T.R., Sharp, J.O., 2020. Changes in surface water quality from small-scale gold mining operations in the Surinamean rainforest. Toxicol. Environ. Chem. 102 (7–8), 334–355. https://doi.org/10.1080/02772248.2020.1792908.
Liang, Y., Yi, X., Dang, Z., Wang, W., Luo, H., Tang, J., 2017. Heavy metal contamination and health risk assessment in the vicinity of a tailing pond in Guangdong, China. Int. J. Environ. Res. Publ. Health 14, 1557.
Malone, A., Smith, N.M., Zeballos Zeballos, E.Z., 2021. Coexistence and conflict between artisanal mining, fishing and farming in a Peruvian boomtown. Geoforum 120, 142–154.
Maree, J.P., du Plessis, P., 1994. Neutralization of acid mine water with calcium carbonate. Water Sci. Technol. 29 (9), 285–296.
Medina, L., Gomez, H., Santos, B., Moreno, J., Pari, W., 2021. Estudio geoambiental en la Cuenca del rio Ocoña. Instituto Geológico Minero y Metalúrgico Boletín Serie N: Línea de Base Geoambiental 2, 222.
Ministerio del Ambiente, 2017. Aprueban Estándares de Calidad Ambiental (ECA) para Agua y establecen Disposiciones Complementarias. Decreto Supremo No 004-2017-MINAM, p. 10.
Morel, B., Durand, P., Jaffrezic, A., Gruau, G., Molenat, J., 2009. Sources of dissolved organic carbon during stormflow in a headwater agricultural catchment. Hydrol. Process. 23, 2888–2901.
Mott, A., Baba, A., Hadi Mosleh, M., Ökten, H.E., Babaei, M., Gören, A.Y., Feng, C., Recepoglu, Y.K., Uzelli, T., Uytun, H., Morata, D., Yükwel, A., Sedighi, M., 2022. Boron in geothermal energy: sources, environmental impacts, and management in geothermal fluid. Renew. Sustain. Energy Rev. 167, 112825.
Munk, L., Faure, G., Pride, D.E., Bigham, J.M., 2002. Sorption of trace metals to an aluminum precipitate in a stream receiving acid rock-drainage; Snake River, Summit County, Colorado. Appl. Geochem. 17 (4), 421–430.
Musolff, A., Schmidt, C., Selle, B., Fleckenstein, J.H., 2015. Catchment controls on solute export. Adv. Water Resour. 86, 133–146.
Nordstrom, D.K., Alpers, C.N., 1999. Geochemistry of acid mine waters. In: Plumlee, G. S., Logsdon, M.J., Filipek, L.F. (Eds.), The Environmental Geochemistry of Mineral Deposits, vol. 6. Rev. Econ. Geol., pp. 133–160
Nordstrom, D.K., Blowes, D.W., Ptacek, C.J., 2015. Hydrogeochemistry and microbiology of mine drainage: an update. Appl. Geochem. 57, 3–16.
O'Neill, J.M., Lund, K., Van Gosen, B.S., Desborough, G.A., Sole, T.C., DeWitt, E.H., 2004. Chapter D1: geologic framework. In: Nimick, D.A., Church, S.E., Finger, S.E. (Eds.), Integrated Investigations of Environmental Effects of Historical Mining in the Basin and Boulder Mining Districts, Boulder River Watershed, Jefferson County, Montana. U.S. Geological Survey Professional Paper 1652-D1, pp. 53–88.
Palacios, C., 2006. Geology of the Explorador Epithermal Vein and Selene Mining District, Apurimac, Peru: Lithostratigraphy, Structure, Alteration and Mineralization. Master Thesis. Colorado School of Mines, Golden, CO, p. 211.
Palacios, C., Dietrich, A., Nelson, E.P., Layer, P.W., 2008. Estilos y control de mineralización en el distrito minero de Selene, Apurímac, Perú (cd-rom). In: Congreso Peruano de Geología 14 & Congreso Latinoamericano de Geología 13. Sociedad Geological del Peru, Resúmenes Lima.
Palacios, S., Alfonso, P., Mata-Perello, J.M., 2011. Caracterización del Yacimiento de Oro de Misky, sur del Peru. Revista de la Sociedad Española de Mineralogía 15, 159–160.

Palacios, S., Alfonso, P., Proenza, J.A., 2014. Mineralogy and geochemistry of the IRG Misky gold deposit, southern Peru. EGU General Assembly 2014 Geophysical Research Abstracts 16, EGU2014–15618.
Plumlee, G.S., 1999. The environmental geology of mineral deposits. In: Plumlee, G.S., Logsdon, M.J., Filipek, L.F. (Eds.), The Environmental Geochemistry of Mineral Deposits, vol. 6. Rev. Econ. Geol., pp. 71–116
Plumlee, G.S., Nash, J.T., 1995. Geoenvironmental models of mineral deposits – fundamentals and applications. In: Bray, du (Ed.), Preliminary Compilation of Descriptive Geoenvironmental Mineral Deposit Models, vols. 95–831. U.S. Geological Survey Open-File Report, pp. 1–9.
Plumlee, G.S., Smith, K.S., Montour, M.R., Ficklin, W.H., Mosier, E.L., 1999. Geologic controls on the composition of natural waters and mine waters draining diverse mineral-deposit types. In: Plumlee, G.S., Logsdon, M.J., Filipek, L.F. (Eds.), The Environmental Geochemistry of Mineral Deposits, vol. 6. Rev. Econ. Geol., pp. 373–432
Pokrovsky, O.S., Viers, J., Emnova, E.E., Kompantseva, E.I., Freydier, R., 2008. Copper isotope fractionation during its interaction with soil and aquatic microorganisms and metal oxy(hydr)oxides: possible structural control. Geochem. Cosmochim. Acta 72, 1742–1757.
Quang, C.X., Clark, A.H., Lee, J.K.W., Guillen, B.J., 2003. ^{40}Ar-^{39}Ar ages of hypogene and supergene mineralization in the Cerro Verde-Santa Rosa Porphyry Cu-Mo cluster, Arequipa, Peru. Econ. Geol. 98 (8), 1683–1696.
Quispe, J., Carlotta, V., Acosta, J., Machare, J., Chirif, H., Rivera, R., Romero, D., Huanacuni, D., Rodríguez, R., 2008. Mapa Metalogenético del Peru 2008. CD Resúmenes del XIV Congreso peruano de Geología Código C-27.
Regis, A., Vanneste, J., Acker, S., Martinez, G., Quea, J., Garcia, V., Alejo, F., Zea, J., Krahenbuhl, R., Vanzin, G., Sharp, J., 2022. Pressure-driven membrane processes for boron and arsenic removal: pH and synergistic effects. Desalination 522, 115441. https://doi.org/10.1016/j.desal.2021.115441.
Royer, T.V., David, M.B., 2005. Export of dissolved organic carbon from agricultural streams in Illinois, USA. Aquat. Sci. 67, 465–471.
Sanchez-España, J., López-Pamo, E., Santofimia, E., Reyes, J., Martín, J.A., 2006. The removal of dissolved metals by hydroxysulphate precipitates during oxidation and neutralization of acid mine waters, Iberian Pyrite Belt. Aquat. Geochem. 12 (3), 269–298.
Santi, P., Manning, J., Zhou, W., Meza, P., Colque, P., 2021. Geologic hazards of the Ocoña river valley, Peru and the influence of small-scale mining. Nat. Hazards 108, 2679–2700.
Santos, A., Weimin, G., Rivera, F., Tassinari, C., Cerpa, L., Kojima, S., 2019. Early Jurassic arc related magmatism associated with porphyry copper mineralization at Zafranal, southern Peru unraveled by zircon U-Pb ages. Andean Geol. 46 (3), 445–470.
Shackleton, R.M., Ries, A.C., Coward, M.P., Cobbold, P.R., 1979. Structure, metamorphism and geochronology of the Arequipa Massif of costal Peru. J. Geol. Soc. Lond. 136, 195–214.
Smith, K.S., 1999. Metal sorption on mineral surfaces: an overview with examples relating to mineral deposits. In: Plumlee, G.S., Logsdon, M.J., Filipek, L.F. (Eds.), The Environmental Geochemistry of Mineral Deposits, vol. 6. Rev. Econ. Geol., pp. 161–182
Smith, N.M., 2019. "Our gold is dirty, but we want to improve": challenges to addressing mercury use in artisanal and small-scale gold mining in Peru. J. Clean. Prod. 222, 646–654.
Smith, K.S., Balistrieri, L.S., Todd, A.S., 2015. Using biotic ligand models to predict metal toxicity in mineralized systems. Appl. Geochem. 57, 55–72. https://doi.org/10.1016/j.apgeochem.2014.07.005.
Strobel, B.W., Hansen, H.C.B., Borggaard, O.K., Andersen, M.K., Raulund-Rasmussen, K., 2001. Cadmium and copper release kinetics in relation to afforestation of cultivated soil. Geochem. Cosmochim. Acta 65 (8), 1233–1242.
Sucapuca, C., 2019. Caracterización petromineralógica de tres yacimientos epitermales del sur peruano. Instituto Geológico Minero y Metalúrgico Boletín Boletín Serie B: Geología Económica 58, 163.
Sunda, W.G., Hanson, P.J., 1979. Chemical speciation of copper in river water. Chem. Model. Aqueous Syst. ACS Symp. Ser. (Am. Chem. Soc.) 8, 147–180. Washington, DC.
Temminghoff, E.J.M., Van der Zee, S.E.A.T.M., De Haan, F.A.M., 1997. Copper mobility in a copper-contaminated sandy soil as affected by pH and solid and dissolved organic matter. Environ. Sci. Technol. 31, 1109–1115.
The International Network for Acid Prevention (INAP), 2009. Global Acid Rock Drainage Guide (GARD Guide). http://www.gardguide.com/. (Accessed 21 July 2022).
Thompson, S.E., Basu, N.B., Lascurain Jr., J., Aubeneau, A., Rao, P.S.C., 2011. Relative dominance of hydrologic versus biogeochemical factors on solute export across impact gradients. Water Resour. Res. 47, W00J05.
U.S. Environmental Protection Agency, 2000. Practical Methods for Data Analysis. U.S. Environmental Protection Agency Office of Environmental Information, Washington, DC, p. 219. EPA QA/G-9, EPA/600/R-96/084.
U.S. Environmental Protection Agency, 2007. Aquatic Life Ambient Freshwater Quality Criteria – Copper 2008 Revision, EPA-822-R-07-001. U.S. Environmental Protection Agency Office of Water, Washington, DC, p. 204.
U.S. Environmental Protection Agency, 2009. Statistical Analysis of Groundwater Monitoring Data at RCRA Facilities – Unified Guidance, EPA 530/R-09-007. U.S. Environmental Protection Agency Office of Resource Conservation and Recovery, p. 888.
Vargas, V., Cruz, V., 2010. Geothermal map of Perú. Proceedings World Geothermal Congress 2010 Bali, Indonesia, April 25-29, p. 6.
Villavicencio, G., Urrestarazu, P., Carvajal, C., De Schamphelaere, K.A.C., Janssen, C.R., Torres, J.C., Rodriguez, P.H., 2005. Biotic ligand model prediction of copper toxicity to Daphnids in a range of natural waters in Chile. Environ. Toxicol. Chem. 24 (5), 1287–1299.
Webster, J.G., Nordstrom, D.K., 2003. Geothermal Arsenic – the source, transport and fate of arsenic in geothermal systems. In: Welch, A.H., Stollenwerk, K.G. (Eds.), Arsenic in Groundwater Geochemistry and Occurrence. Kluwer Academic Publishers, pp. 101–125.
Yager, D.B., 2008. Chapter K: environmental rock properties at abandoned mine lands that generate or neutralize acid drainage, silverton, Colorado. In: Verplacnk, P.L. (Ed.), Understanding Contaminants Associated with Mineral Deposits, vol. 1328. U. S. Geological Survey Circular, pp. 64–69.
Yager, D.B., McCafferty, A.E., Stanton, M.R., Diehl, S.F., Driscoll, R.L., Fey, D.L., Sutley, S.J., 2005. Net Acid Production, Acid Neutralizing Capacity, and Associated Geophysical, Mineralogical, and Geochemical Characteristics of Animas River Watershed Rocks Near Silverton, Colorado, vols. 2005–1433. U.S. Geological Survey Open-File Report, p. 75.
Yang, Z., Acker, S.M., Brady, A.R., Arenazas, A., Morales, L., Ticona, J., Romero, G., Vanzin, G.F., Ranville, J.F., Sharp, J.O., 2023. Heavy metal removal by the photosynthetic microbial biomat found within shallow unit process open water constructed wetlands. Sci. Total Environ. 876, 162478 https://doi.org/10.1016/j.scitotenv.2023.162478.
Ye, Z., Mao, J., Lu, M., Zhu, Z., Chen, N., Wei, H., Jin, W., Meng, Z., 2022. Geology and geochronology of the Don Javier Cu-Mo porphyry deposit, southern Peru. Ore Geol. Rev. 143, 104777.